PABERFIA – Lightweight sandwich panels in steel fiber reinforced self compacting concrete

Report 05-DEC/E-21

Research team:

Joaquim Barros, Depart. Engª Civil, Escola de Engª, Universidade do Minho, barros@civil.uminho.pt;
Eduardo Pereira, Depart. Engª Civil, Escola de Engª, Universidade do Minho, epereira@civil.uminho.pt;
Vítor Cunha, Depart. Engª Civil, Escola de Engª, Universidade do Minho, vcunha@civil.uminho.pt;
Alberto Ribeiro, Civitest - pesquisa de novos materiais para a engenharia civil, Lda., alberto@civil.uminho.pt;
Simão Santos, Civitest - pesquisa de novos materiais para a engenharia civil, Lda., simaopfsantos@civitest.pt;
Paulo Queirós, PRÉGAIA, Sociedade de Pré-Fabricação, S.A., pqueiros@pregaia.com

Date: October 2005
N.º of pages: 63

Departamento de Engenharia Civil da Escola de Engenharia

Universidade do Minho

CiviTest - Pesquisa de novos materiais para a Engenharia Civil, L.da

Prégaia – Sociedade de Pré-Fabricação, S.A.

Azurém, 4800-085 Guimarães - Tel. 253 510 200 - Fax 253 510 217 - E-mail secG@civil.uminho.pt

"PABERFIA – LIGHTWEIGHT SANDWHICH PANELS IN STEEL FIBER REINFORCED SELF COMPACTING CONCRETE"

Report of PABERFIA Project, financed by operational programs Science, Technology and Innovation (POCTI) and Information Society (POSI) co participated by FEDER and National Funds of MCT.

We would like to thank the following institutions:

FCT – Fundação para a Ciência e a Tecnologia; ADI – Agência de Inovação; BEKAERT; Degussa Chemicals Portugal; COMITAL – Companhia Mineira de Talcos, SA; SECIL – Companhia geral de cal e cimento, SA; DuroEuropa – Produtos Endurecedores, Lda; Marques e Cruz, Lda and FiberSensing.

Index

Figure Index

Table Index

1. INTRODUCTION

The concrete precasting industry is frequently confronted with the production of structural reinforced concrete elements of some geometric complexity. These geometric conditions introduce difficulties on the placement of reinforcement, resulting in a large consuming time phase of the industrial process. Moreover, when high percentage of reinforcement is used, there are difficulties on assuring the desired concrete pouring quality, resulting in deficiencies that can compromise the mechanical behavior and the visual appearance of the final structure.

Self-compacting concrete (SCC) can be defined as concrete that is able to flow in the interior of the formwork, passing through the reinforcement and filling it in a natural manner, being consolidated under the action of its own weight. Adding the benefits of SCC to those resulting from the addition of discrete fibers to cement based materials, a high performance material, designated by steel fiber reinforced self-compacting concrete (SFRSCC), is obtained.

The present work is part of a research program for the development of lightweight sandwich SFRSCC panels for building façade applications, to be produced by the pre-casting industry. The requirements established for this SFRSCC were the following: average compression strength at 24 hours greater than 20 MPa; equivalent flexural tensile strength greater than 2 MPa at this age; content of cement not exceeding 400 Kg/m^3; the cement should be the most expensive component of the binder paste. The strategy followed to design this SFRSCC is briefly described in the present report.

In the precasting industry, the ability to demold the elements as soon as possible is an important requirement. To assure safe demolding process, the influence of the concrete age on the flexural and compression behavior of the SFRSCC should be known. For this purpose, an experimental program was carried out with specimens of 12 hours, 24 hours, 3, 7 and 28 days. Special care was taken to evaluate the post-cracking behavior of the SFRSCC, since the fracture mode I crack constitutive law was derived from the results obtained in these flexural tests, and used in a discrete crack model implemented into a computational code based on the finite element method (FEM) that is able of simulating the nonlinear behavior of concrete structures. The experimental program is described and the results are presented and analyzed.

When installed in building façades, the panel's flexural strength is the principal design property since significant bending moments result from wind loading, which has the greatest impact on the most unfavorable load combination. Representative elements of the SFRSCC panel system were tested to

assess its flexural behavior. Since the SFRSCC layer at the lightweight parts of the panel is only 30 mm thick, its resistance to punching was also determined, based on experimental tests.

The research program ended with the fabrication of a real size panel in industrial environment. This panel was loaded up to failure in order to evaluate its load carrying capacity.

2. SELF COMPACTING CONCRETE TECHNOLOGY

2.1. Definition of Self Compacting Concrete

Self-compacting concrete (SCC) can be defined as concrete that is able to flow in the interior of the formwork, passing through the reinforcement and filling it in a natural manner, being consolidated under the action of its own weight. Besides the requirement of being consolidated without the use of any vibration equipment, segregation should not occur during the application of SCC.

The first steps in the self compacting technology of concrete were given in Tóquio University, Japan, in 1986. The first application of SCC in a prototype was made in 1988 (Okamura e Ouchi, 1999). Since then, a great effort has been done in the improvement of the SCC technology and in the characterization of its properties by experimental research.

2.2. Properties of SCC

To assure self-compacting requirements to a concrete, the mixture should have the right values for its fluidity, viscosity and cohesion, in order to assure that the mixture flows homogeneously without the occurrence of segregation. This type of exigencies is not required for conventional concretes. In consequence, specific tests should be carried out to check self-compacting requirements.

The high fluidity of SCC gives it the capacity of flowing within the formwork, filling it only under its own weight. SCC has also the capacity to evolve the spaces between any obstacles. Segregation of the SCC components can be avoided controlling the viscosity and the cohesion of the mixture.

The microstructure and the "inert-binder paste" interface of SCC are more compact than the ones of conventional concrete of same water/binder ratio. In consequence, if compared to conventional concrete, SCC has high resistance to clorets and gases penetration and has also higher adherence to the reinforcement. However, in general, SCC has higher content of cement than conventional concrete, which requires extra cautions during its curing procedure to avoid crack formation, mainly in elements that have some restrictions to its deformation.

2.3. Properties of Steel Fiber Reinforced Self Compacting Concrete

The use of discrete steel fibers as a reinforcement system for cement based materials is a current practice for several applications. The resulting material is designated Steel Fiber Reinforced Concrete (SFRC). The post cracking residual stress is much higher in SFRC than in plain concrete (PC), due to fiber reinforcement mechanisms provided by fibers bridging the cracks. In consequence, SFRC allows high level of stress redistribution, providing a significant deformability capacity of a structure between crack initiation and its failure, which increases the structural safety. This is especially relevant in structures of a redundant number of supports. The level of the post cracking residual stress depends of several factors, namely: fiber geometric characteristics, fiber material properties, concrete properties, method of SFRC application.

The benefits provided by concrete fiber addition are also visible in structures submitted to cyclic and fatigue loads, since this material can be engineered to have very high energy absorption capacity. When well conceived, fiber reinforcement can replace totally or partially conventional steel reinforcement for the flexural and shear resistance of concrete elements. The percentage of this replacement depends on the type of element, and support and loading conditions.

Adding the benefits that fiber reinforcement can provide to those resulting from the characteristics of self-compacting, a high performance material can be obtained, designated Steel Fiber Reinforced Self-Compacting Concrete (SFRSCC).

2.4. Phases of SCC development

SCC can be seen as a material constituted of a solid and a fluid phase.

The solid phase is composed by the solid skeleton of the mixture, being constituted by the aggregates of an equivalent diameter larger than 150 μm. The research involving the solid skeleton should have the purpose of obtaining the highest compact skeleton.

The fluid phase (binder paste) has the main function of transporting the concrete constituent particles in a stable and cohesive way. This phase is composed by water, adjuvants and a solid part of particles of an equivalent diameter smaller than 150 μm. This phase is the most complex of the mixture, due to the diversity and the nature of its components.

Superplasticizers have the function of dispersing the particles and avoid flocculation.

These flakes appeared in the sequence of the aggregation of particles in suspension, resulting greater spaces between particles and a reduction on the paste fluidity. To fulfill the space in-between particles the content of the water should increase.

2.5. Tests to assess Self Compacting requisites

The most common tests to assess the self compacting requirements are the following: V-Funnel, L-Box and Slump Flow. Some of them can also be associated: Slump Flow with J-Ring or J-Ring with U-Box. These tests, providing values in length and time unities, can decide about considering, or not, a concrete as a SCC. They are easy of executing and do not require to build sophisticate and expensive apparatus. The values provided by these tests have empirical basis.

2.5.1. Slump Flow

The slump flow test is used to assess the horizontal free flow of SCC in the absence of obstructions. It was first developed in Japan for use in assessment of underwater concrete. The test method is based on the Abrams Cone test, which is the most used to assess the workability and fluidity of fresh concrete. It can also detect, by visualization, the occurrence of segregation. The diameter of the concrete circle is a measure for the filling ability of the concrete.

The characteristics of the instruments are specified in EN 12350-2 and ISO 4109 standards. The inferior and superior bases of the Abrams Cone has 200 mm and 100 mm diameter, respectively, while its height has 300 mm height. In a steel base plate, two concentric circumferences are marked, one with 200 mm of diameter and the other with 500 mm of diameter (see Figures 2.1 and 2.2).

Figure 2.1: Abrams Cone

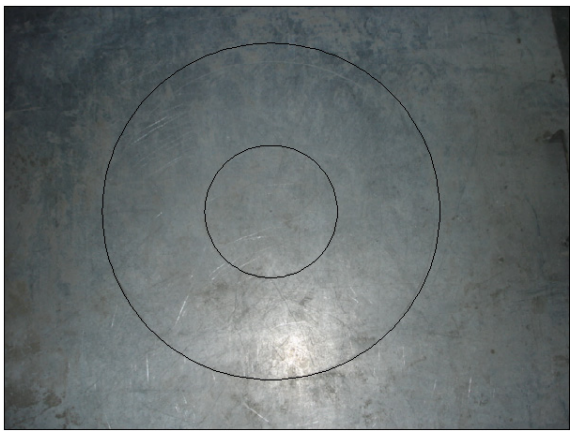

Figure 2.2: Base to perform the test

The higher the slump flow (d_f) value, the greater its ability to fill formwork under its own weight. A value of *at least* 650mm is required for SCC. There is no generally accepted advice on what are reasonable tolerances about a specified value, though ± 50mm, as with the related flowtable test, might be appropriate.

The T50 time is a secondary indication of flow. A lower time indicates greater flowability. The *Brite EuRam* research suggested that a time of 3-7 seconds is acceptable for civil engineering applications, and 2-5 seconds for housing applications.

Figure 2.3: Measuring the final diameter of SFRSCC

In case of severe segregation most coarse aggregate will remain in the centre of the pool of concrete and mortar and cement paste at the concrete periphery. In case of minor segregation a border of mortar without coarse aggregate can occur at the edge of the pool of concrete. If none of these phenomena appear it is no assurance that segregation will not occur since this is a time related aspect that can occur after a longer period.

Abrams Cone with J-Ring

To assess the fluidity of SCC, when it should be passed through steel bars in RC elements, a combination of Abrams Cone and J-Ring is used, placing the Abrams Cone inside the J-Ring (see Figures 2.4 and 2.5). The principle of the J-Ring test may be Japanese, but no references are known. The J-Ring test itself has been developed at the University of Paisley. The test is used to determine the passing ability of the concrete. The equipment consists of a rectangular section (30mm x 25mm) open steel ring, drilled vertically with holes to accept threaded sections of reinforcement bar. These sections of bar can be of different diameters and spaced at different intervals: in accordance with normal reinforcement considerations, 3x the maximum aggregate size might be appropriate. The diameter of the ring of vertical bars is 300mm, and the height 100 mm.

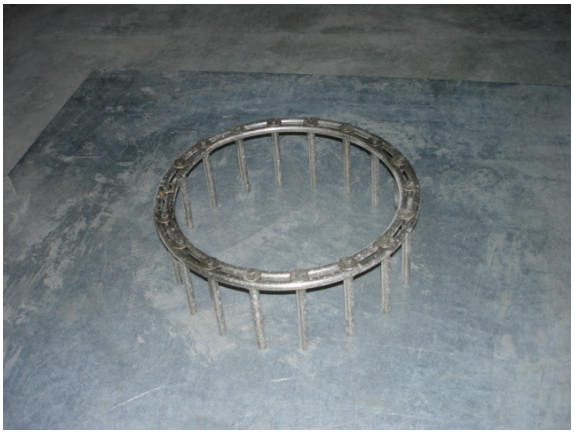

Figure 2.4: J-Ring

Figure 2.5: Combination of J-Ring with Abrams Cone

2.5.2. L-Box

This test, based on a Japanese design for underwater concrete (Petersson *et al.*, 1996; Bartos and Grauers, 1999). The test assesses the flow of the concrete, and also the extent to which it is subject to blocking by

reinforcement. The apparatus is shown in Figure 2.6. The apparatus consists of a rectangular-section box in the shape of an 'L', with a vertical and horizontal section, separated by a moveable gate, in front of which vertical lengths of reinforcement bar are fitted. The vertical section is filled with concrete, then the gate lifted to let the concrete flow into the horizontal section.

Figure 2.6: L-Box

When the flow has stopped, the height of the concrete at the end of the horizontal section is expressed as a proportion of that remaining in the vertical section H2/H1 (see Figures 2.7, 2.8 and 2.9). It indicates the *slope* of the concrete when at rest. This is an indication passing ability, or the degree to which the passage of concrete through the bars is restricted. The horizontal section of the box can be marked at 200mm and 400mm from the gate and the times taken to reach these points measured. These are known as the T20 and T40 times and are an indication for the filling ability. The sections of bar can be of different diameters and spaced at different intervals: in accordance with normal reinforcement considerations, 3x the maximum aggregate size might be appropriate. The bars can principally be set at any spacing to impose a more or less severe test of the passing ability of the concrete.

Figure 2.7: End of test

Figure 2.8: Measuring h2

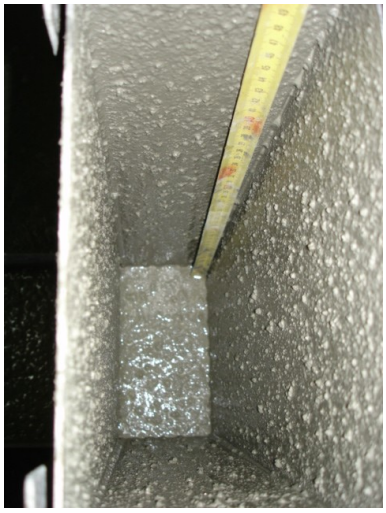

Figure 2.9: Measuring h1

If the concrete flows as freely as water, at rest it will be horizontal, so H2/H1 = 1. Therefore the nearer this test value, the 'blocking ratio' (C_{bl}), is to unity, the better the flow of the concrete. The EU research team suggested a minimum acceptable value of 0.8. T20 and T40 times can give some indication of ease of flow, but no suitable values have been generally agreed. Obvious blocking of coarse aggregate behind the reinforcing bars can be detected visually as well as the occurrence of segregation can also be visualized in qualitative manner.

2.5.3. U-Box

The test was developed by the Technology Research Centre of the Taisei Corporation in Japan (Rooney, M., Bartos, P.M.J, 2001). Sometimes the apparatus is called a "box-shaped" test. The test is used to measure the filling ability of self-compacting concrete. The apparatus consists of a vessel that is divided by a middle wall into two compartments (see Figure 2.10). An opening with a sliding gate is fitted between the two sections. Reinforcing bars with nominal diameters of 13 mm are installed at the gate with centre-to-centre spacing of 50 mm. This creates a clear spacing of 35 mm between the bars. The left hand section is filled with about 20 litre of concrete then the gate lifted and concrete flows *upwards* into the other section. The height of the concrete in both sections is measured.

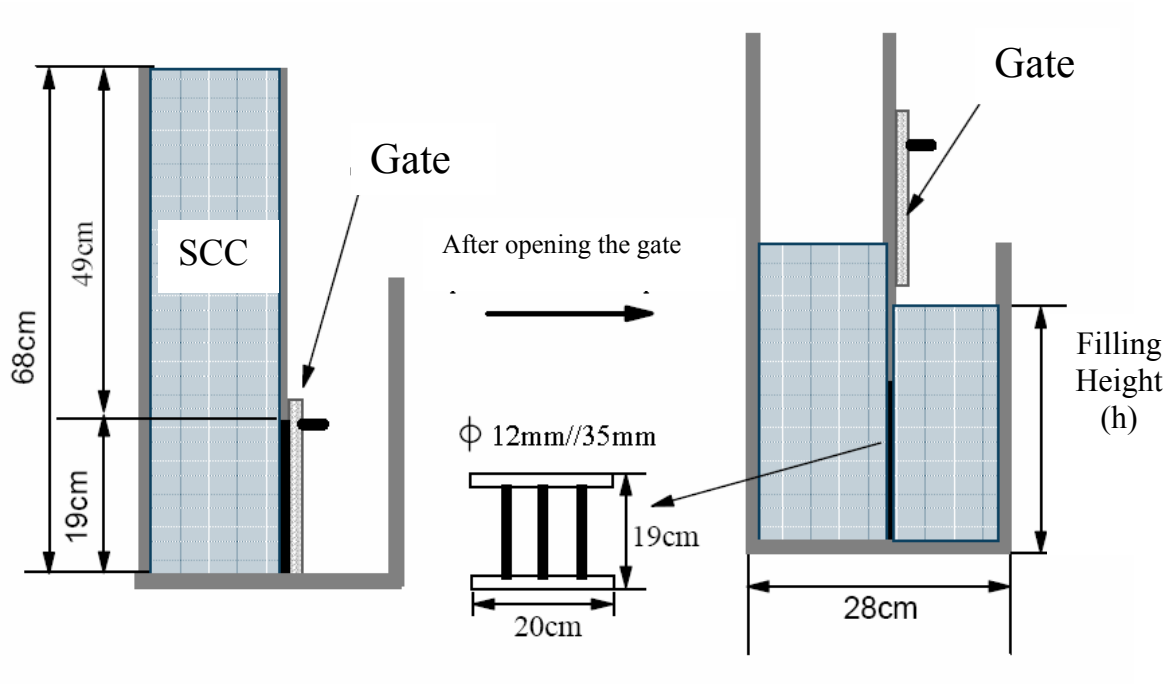

Figure 2.10: U-Box

If the concrete flows as freely as water, at rest it will be horizontal, so H1-H2 = 0. Therefore the nearer this test value, the 'filling height', is to zero, the better the flow and passing ability of the concrete.

2.5.4. V-Funnel

The test was developed in Japan and used by Ozawa et al in the University of Tokyo(Gomes, 2002). The equipment consists of a V-shaped funnel, shown in Figure 2.11. An alternative type of V-funnel, the O funnel, with a circular section is also used in Japan. The described V-funnel test is used to determine the filling ability (flowability) of the concrete with a maximum aggregate size of 20mm. The funnel is filled with about 12 litre of concrete and the time taken for it to flow through the apparatus measured. After this the funnel can be refilled concrete and left for 5 minutes to settle. If the concrete shows segregation then the flow time will increase significantly.

Figure 2.11: V-Funnel

This test measures the ease of flow of the concrete; shorter flow times indicate greater flowability. For SCC a flow time of 10 seconds is considered appropriate. The inverted cone shape restricts flow, and prolonged flow times may give some indication of the susceptibility of the mix to blocking. After 5 minutes of settling, segregation of concrete will show a less continuous flow with an increase in flow time.

3. EXPERIMENTAL PROGRAMS

3.1. Experimental Program I – SFRSCC_30

3.1.1. Conception method

The used materials were cement (C) CEM I 42.5R, limestone filler (LF), superplasticizer (SP) of third generation based on polycarboxilates (Glenium® 77SCC), water (W), three types of aggregates (fine river sand, coarse river sand and crushed granite 5-12 mm) and DRAMIX® RC-80/60-BN hooked end steel fibers. This fiber has a length (l_f) of 60 mm, a diameter (d_f) of 0.75 mm, an aspect ratio (l_f/d_f) of 80 and a yield stress of 1100 MPa. The method developed in the present work is based on the three following steps: i) the proportions of the constituent materials of the binder paste are defined; ii) the proportions of each aggregate on the final solid skeleton are determined; iii) binder paste and solid skeleton are mixed in different proportions until self-compacting requirements in terms of spread ability, correct flow velocity, filling ability, blockage and segregation resistance are assured.

In the first step, a series of tests were performed to achieve the optimum composition of the binder paste. To define the optimum percentage of LF addition in the final composition, several mixes of LF, cement and water were prepared. The proportions of each component were defined in terms of volume, the water content was 66% of cement volume, and the percentage of LF has varied between 0% and 125% of the cement volume. To promote the dispersion and deflocculation of the fine particles in suspension, a small constant quantity of superplasticizer was also added to each mix. The relative spread in the "Flow table" and the “Marsh cone” flow time of each mix were measured. Concluding the paste phase design, the compression strength of each mix was also evaluated on 5 cm edge cubic specimens at an age of 7 days. A percentage of 100% of LF relative to the cement volume has resulted in a good compromise between strength and flowability requirements, and has also allowed maintaining the amount of cement on the final concrete mix only slightly above 350 kg/m^3.

In the second step, the most appropriate proportions of the three types of aggregates were obtained preparing mixes of distinct quantities of each type of aggregate, and weighting 5 dm^3 volume for each mix. The optimum aggregate mix was assumed to be the heaviest one, since it should correspond to the most compact. An estimated portion of fibers equivalent to 30 Kg of fibers per m^3 of concrete was included in each mixture. Initially, only two of the three types of aggregates were mixed. After finding the optimum relation between these two, the third aggregate was added in distinct volumetric percentages,

keeping constant the relation between the two first aggregates. These results indicated that the optimum solid skeleton was composed, in volume, by 49.5% of coarse sand, 40.5% of crushed stone and 10% of fine sand.

The third phase is dedicated to the evaluation of the paste content in the concrete volume. The optimum composition should accomplish an upper limit of around 350 kg of cement per m^3 of concrete. To achieve the optimum paste content, some mixes of concrete were prepared, varying the paste percentage. For each mix, the added water was evaluated taking into account the aggregate's saturation degree. The mix process was always the same, and for each mix the slump flow test was performed. Total spread, d_f, and time to reach a spread diameter of 500 mm, T_{50}, were measured. Table 1 includes the composition that has best fitted self-compacting requirements (the amount of water referred includes the aggregate's saturation water). No sign of segregation was detected, a total spread of 725 mm was measured and the mixture showed good homogeneity and cohesion, even when flowing trough the small orifice of the Abrams cone (when testing, Abrams cone was always used in the inverted position). A T_{50} of 4.6 seconds was measured.

Table 3.1: Final Composition for 1 m^3 of SFRSCC 30 kg of fibers

Paste/Total volume (%)	Cement (kg)	LF (kg)	Water (dm^3)	SP (dm^3)	Fine sand (kg)	Coarse sand (kg)	Crushed aggregates (kg)
0.34	364.28	312.24	139.12	6.94	108.59	723.96	669.28

3.1.2. Mechanical Properties of SFRSCC

3.1.2.1. Compression

The experimental program was composed by uniaxial compression tests with cylinders of 150 mm diameter and 300 mm height, and flexural tests with prismatic 600×150×150 mm^3 specimens. Both types of specimens were molded without any external compaction. To assess the influence of the age of SFRSCC on the compression and on the flexural behavior, series of tests with specimens of 12 and 24 hours, and 3, 7 and 28 days were carried out.

The Young Modulus (Ec) is determined according to the recommendations of the LNEC E397-1993 standard, using the test setup represented in Figure 3.1. This test setup is composed by two rings at 100mm from each other. In the superior ring three LVDTs (Linear Variation Displacement Transducer) are placed, making an angle of 120º between them. These LVDTs read the deformation of the concrete

specimen between the two rings. This proceeding avoids that the LVDTS register extraneous deformations.

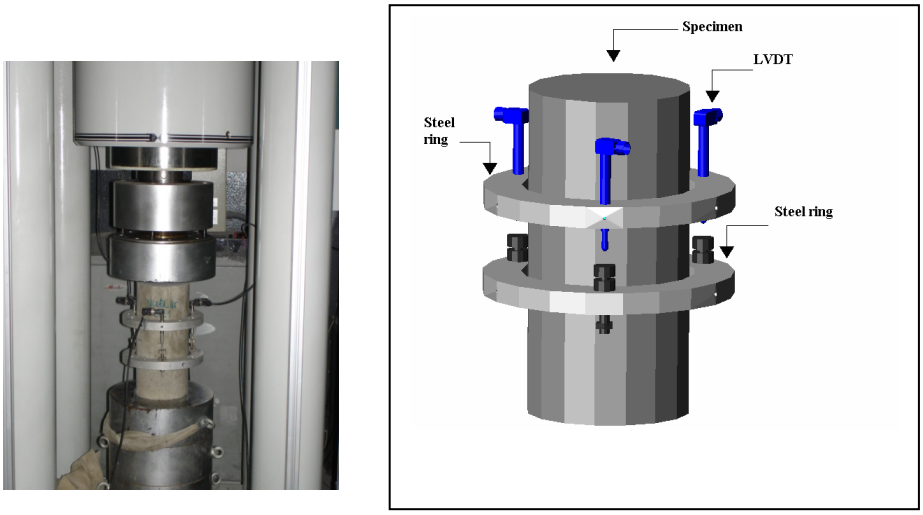

Figure 3.1 Test setup to evaluate the concrete Young's Modulus, E_c

To start the test, a stress of 0.5 to 1 MPa (σ_b) is applied, and the corresponding strain is measured (ε_b). The stress is than increased at a velocity of 0.5 ± 0.1 MPa/s until a stress level $\sigma_a = f_c / 3$ is reached, where f_c is the compressive strength, previously obtained in direct compression tests with concrete cylinder specimens. The stress σ_a is maintained during 90 seconds, and in the last 30 seconds of this period, the strains are recorded (ε_{a1}). After this period, the load is decreased at a stress ratio of 0.5 ± 0.1 MPa/s until a stress level σ_b. This stress level is maintained during a period of 90 seconds, and in the last 30 seconds of this period, the strains are recorded. The loading configuration of this test is composed of 10 cycles of this type, see Figure 3.2.

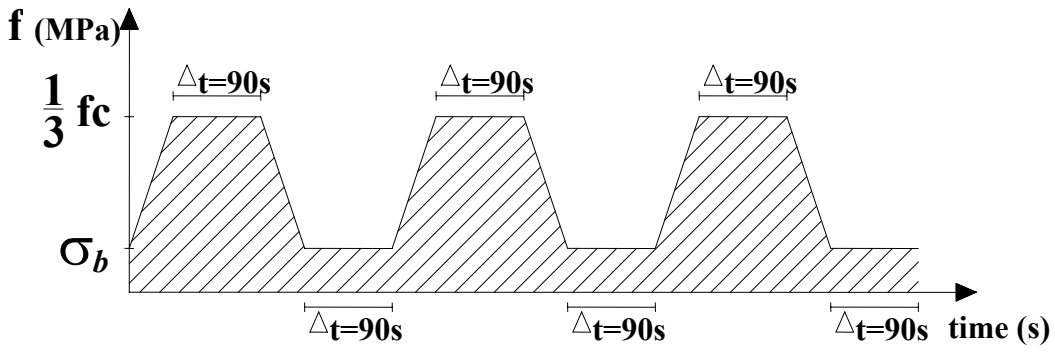

Figure 3.2: Representation of load cycles to determine Ec

The Young's Modulus, E_{cm}, is the average of the $E_{c,n}$ values obtained in each cyclic:

$$E_{c,n} = \frac{\Delta\sigma_n}{\Delta\varepsilon_n} = \frac{\sigma_{a,n} - \sigma_{b,n}}{\varepsilon_{a,n} - \varepsilon_{b,n}} \quad (1)$$

where $\sigma_{a,n}$ and $\sigma_{b,n}$ are the average stress of the nth cyclic, and $\varepsilon_{a,n}$ and $\varepsilon_{b,n}$ are the corresponding strains.

Compression tests were carried out in a servo-controlled equipment of 3000 kN maximum load carrying capacity. Each test was controlled by the internal displacement transducer of this equipment, at a displacement rate of 5 μm/s. Three displacement transducers were positioned at 120 degrees around the specimen to record the displacements between the load steel plates of the equipment, see Figure 3.3. This arrangement of the LVDTs avoids that extraneous deformations, such as the deformation of the reaction frame, are added to the values recorded by the LVDTs.

Taking the values recorded in these transducers, the displacement at the specimen axis was determined for each scan reading, and the corresponding strain was obtained dividing this displacement by the measured specimen's height.

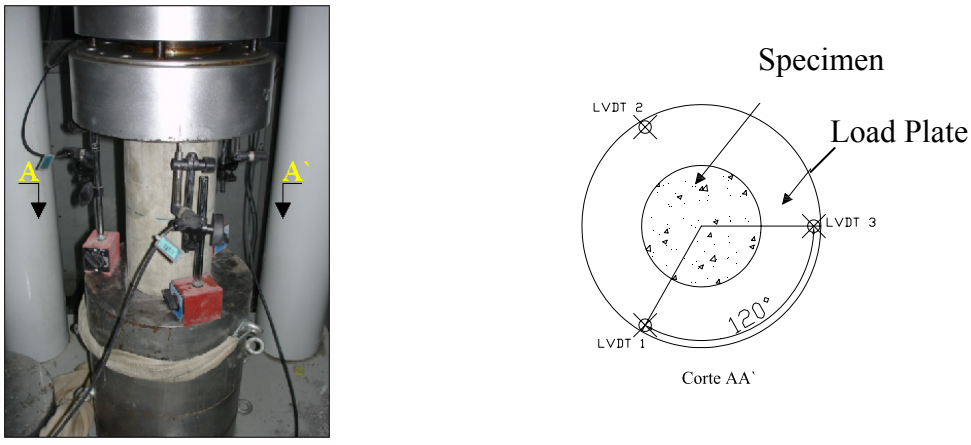

Figure 3.3: Configuration of compression test and position of the LVDTs

The compression stress-strain relationship, $\sigma_c - \varepsilon_c$, for each testing age of SFRSCC is represented in Figure 3.4. Each curve is the average of three specimens. As it was expected, the decay of the post-peak residual compression strength has increased with the SFRSCC age, since the material becomes more brittle with the increase of the compressive strength. However, this decay is not as pronounced as it will be expected for plain concrete.

Figure 3.5 checks if the $\sigma_c - \varepsilon_c$ expressions proposed by Model Code CEB-FIP 1993 to simulate the uniaxial compression behavior of plain concrete can be applicable to the developed SFRSCC. This figure shows that those expressions simulate with high accuracy the uniaxial compression behavior of the designed SFRSCC up to its peak stress, but in the softening phase (post-peak) they predict a stress decay higher than the one observed experimentally.

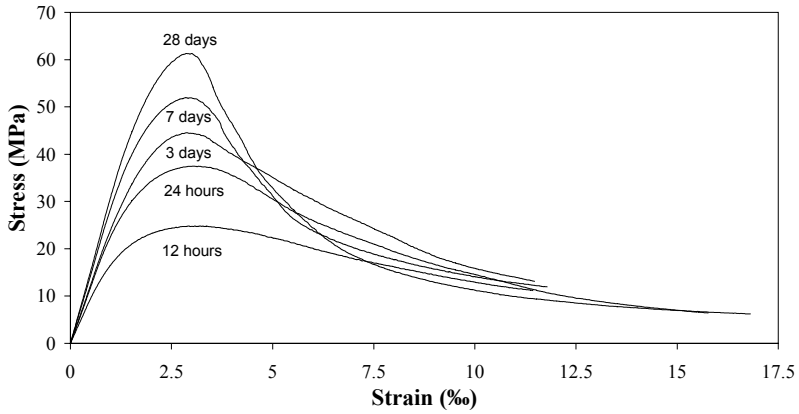

Figure 3.4: Stress-strain curves of SFRCSCC of different ages.

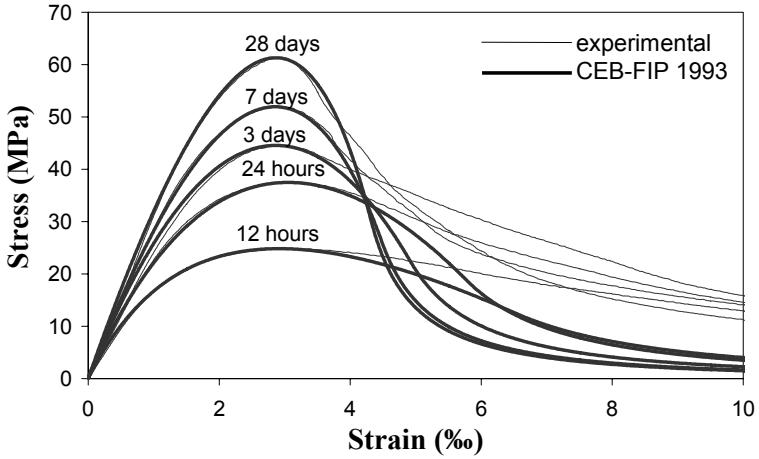

Figure 3.5: Evaluation of the applicability of CEB-FIP 1993 expressions to simulate the behavior of SFRSCC in uniaxial compression.

Figures 3.6 and 3.7 show the influence of the age on the average compressive strength, f_{cm}, and on the average initial Young's Modulus, E_{cm}. From the analysis of these figures, the following observations can be pointed out: at 12 hours the pre-established minimum limit of 20 MPa for the compressive strength at 24 hours had already been exceeded. At this age the f_{cm} was about 25 MPa while the E_{cm} was around

24 GPa. These properties increased with the SFRSCC age, reaching f_{cm} = 62 MPa and E_{cm} = 36 GPa at 28 days. The evolution of the compressive strength with time indicates that, above 28 days the increase of f_{cm} is marginal. This can be justified by the use of relatively high percentage of a material (limestone filler) without pozolanic activity in the binder paste composition. The evolution of the Young's Modulus with the age indicates that above 28 days the increase of the E_{cm} is marginal. This can be justified by the low value of the water/cement ratio (approximately 0.28 in weight), since a high compact matrix has resulted. At 24 hours the f_{cm} and the E_{cm} were about 61% and 79% of the corresponding values at 28 days. In the first hours, there was a more pronounced increase in E_{cm} than in f_{cm}.

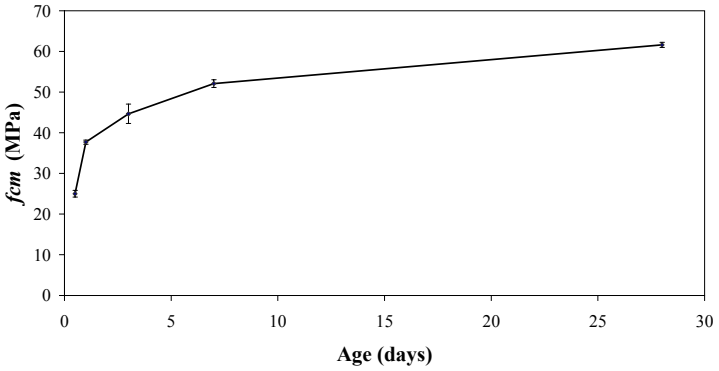

Figure 3.6: Variation of f_{cm} with age.

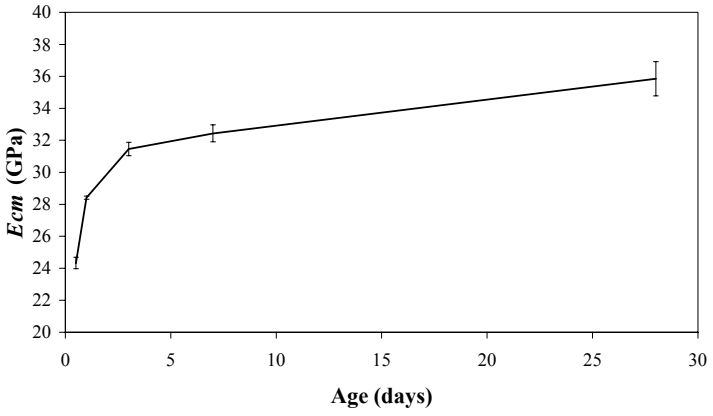

Figure 3.7: Variation of E_{cm} with age.

3.1.2.2. Bending

3.1.2.2.1 Concepts

In the bending tests, the curing procedures, the position and dimensions of the notch sawn into the specimen, the load and specimen support conditions, the characteristics for both the equipment and measuring devices and the test procedures recommended by RILEM TC 162-TDF were adopted. The method for casting the beam specimens proposed by RILEM TC 162-TDF was adapted for SFRSCC since they were cast without any external compaction energy.

RILEM TC 162-TDF recommends the use of 600 ×150×15 mm^3 beams, with a notch of 2-3 mm thick and 25±1 mm depth at the specimen middle surface. The test setup is represented in Figure 3.8. At the notch mouth a "clip gauge" can be applied to measure the crack opening.

The LVDT is attached to a bar that is supported in two fixed points of the specimen. The bar may rotate in turn of one of these points and slide along the other one (Figure 3.8d). This arrangement for the support of the LVDT is designated by "Yoke system" (Gopalaratnam et al. 1991) and avoids extraneous deflections to be read by the LVDT. The reaction frame must have enough stiffness to avoid the occurrence of unstable tests (Hordijk 1991).

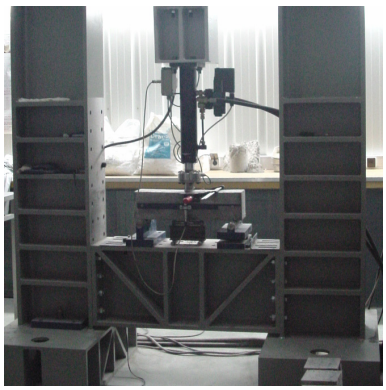

a)

b)

c)

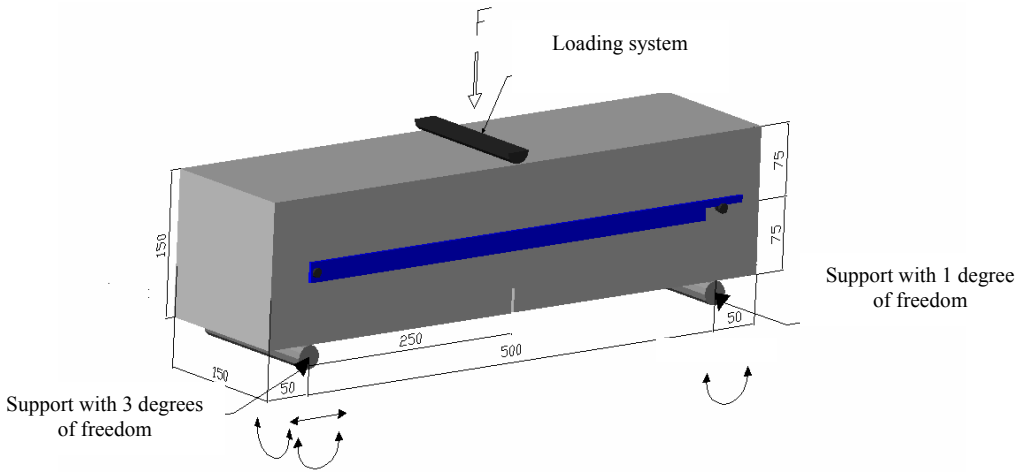

d)

Figure 3.8: Bending Test Setup

The quality of the controller equipment and the stiffness of the reaction structure used in this project, allow performing stable tests under displacement control. The load cell, with maximum load capacity of 50 kN, has a linearity class of 0.03% of full scale. The LVDT presents a linearity class of 0.1% of full scale (5 mm) and a repeatability of 0.01% of full scale.

The crack must start in the notch; otherwise the test must be rejected. The test is carried out at a deflection ratio of 0.2 mm/min. The test ends when a displacement of 3.1 mm is reached.

Figure 3.9 represents a typical force-deflection (F-δ) relationship obtained in a bending test. Using these relationships, RILEM TC 162-TDF proposed the evaluation of the load at the limit of proportionality (F_L), the equivalent ($f_{eq,2}$ and $f_{eq,3}$) and the residual ($f_{R,1}$ and $f_{R,4}$) flexural tensile strength parameters (Vandewalle *et al*. 2000, 2002). F_L is the highest value of the load recorded up to a deflection of 0.05 mm.

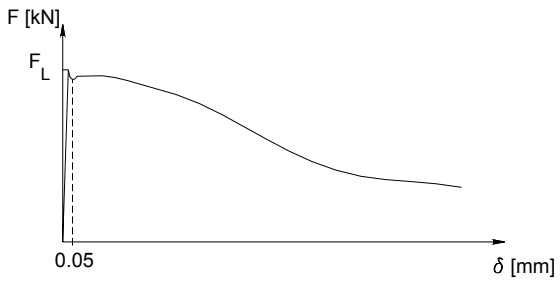

(a)

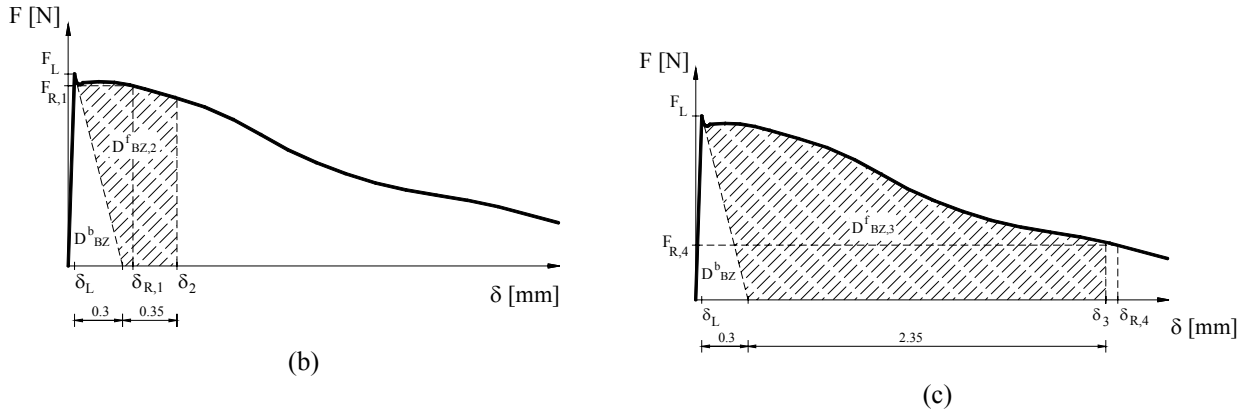

Figure 3.9: Normal Load-Displacement relation in a bending test

The parameters $f_{eq,2}$ and $f_{eq,3}$ are related to the material energy absorption capacity up to a deflection of δ_2 and δ_3 ($\delta_2 = \delta_L + 0.65$mm and $\delta_3 = \delta_L + 2.65$mm, where δ_L is the deflection corresponding to F_L) provided by fibre reinforcement mechanisms ($D^f_{BZ,2}$ and $D^f_{BZ,3}$), as seen in Figure 3.9. The parcel of the energy due to matrix cracking (D^b_{BZ}) is not considered in the f_{eq} evaluation. The parameters $f_{R,1}$ and $f_{R,4}$ are the stresses for the forces $F_{R,1}$ and $F_{R,4}$, respectively, at deflection of $\delta_{R,1}$ = 0.46 mm and $\delta_{R,4}$ = 3.0 mm. Assuming a linear stress distribution in the cross section (see Figure 3.10), the equivalent (Vandewalle *et al*. 2000) and the residual (Vandewalle *et al*. 2002) flexural tensile strength parameters are obtained from the following expressions:

$$f_{eq,2} = \frac{3}{2}\frac{D^f_{BZ,2}}{0.50}\frac{L}{bh^2_{sp}} \;;\; f_{eq,3} = \frac{3}{2}\frac{D^f_{BZ,3}}{2.50}\frac{L}{bh^2_{sp}} \;\; [\text{N/mm}^2] \tag{2}$$

$$f_{R,1} = \frac{3}{2}\frac{F_{R,1}L}{bh^2_{sp}} \;;\; f_{R,4} = \frac{3}{2}\frac{F_{R,4}L}{bh^2_{sp}} \;\; [\text{N/mm}^2] \tag{3}$$

The tensile stress at the limit of proportionality, $f_{fct,fl}$, is obtained from the following expression:

$$f_{fct,ft} = \frac{3}{2}\frac{F_L}{b}\frac{L}{h^2_{sp}} \tag{4}$$

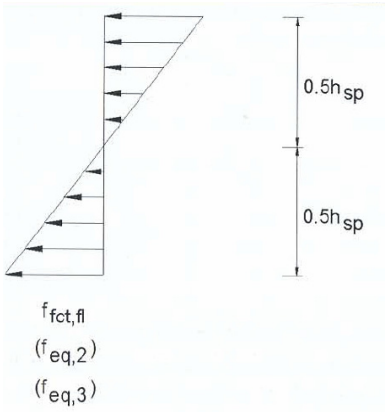

Figure 3.9: Assumed stress distribution in the beam cross section

The parameters $f_{eq,2}$ and $f_{R,1}$ are used on the design at serviceability limit states, while $f_{eq,3}$ and $f_{R,4}$ are used on the design at ultimate limit states (Vandewalle et al. 2000).

3.1.2.2.2 Results

The force-deflection curves, F-δ, obtained in the tested series are depicted in Figure 3.11. Each curve is the average of the F-δ relationship recorded in three specimens. The influence of the SFRSCC age in the force corresponding to the limit of proportionality, F_L, is graphically represented in Figure 3.12. As shown in this figure, F_L increased with the SFRSCC age, but this increase became marginal after 7 days. Just after deflection at midspan value reach δ_L, a load decay occurred with an amplitude that increased with the SFRSCC age (see Figure 3.11), since a higher load should be sustained by the fibers bridging mechanism at the specimen's fracture surface. This load decay was followed by a hardening phase up to a deflection level that has decreased with the SFRSCC age. Except for specimens of 28 days, the maximum load was larger than F_L. Apart series of 12 hours, in the remaining series, the hardening phase was followed by a softening branch. The decrease of residual strength in the softening branch was much more significant in series of specimens with 28 days. The larger amplitude of load decay just after reaching δ_L in this series would have adversely affected the fiber-concrete bond properties and the fiber anchorage efficacy, leading to a decrease in the force necessary to pullout the fibers crossing the specimen fracture surface. As a result, the equivalent (f_{eq}) and the residual (f_R) flexural tensile strength parameters have only decreased between 7 and 28 days, as seen in Figure 3.13. This decrease was more pronounced in the $f_{R,4}$ since this parameter is directly dependent on the shape of the force-deflection curve, and is evaluated for a deflection of 3.0 mm. As $f_{eq,2}$ and $f_{R,1}$ had similar variation with the age, this means that, for low values of deflection (δ_2 and $\delta_{R,1}$), the energy and the force based concepts provide identical results.

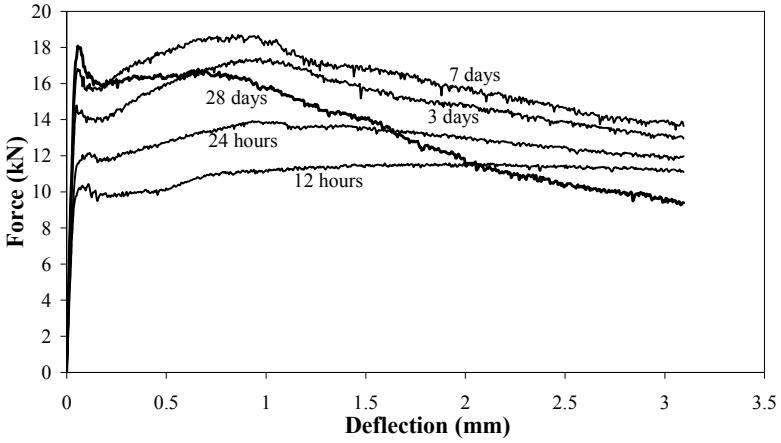

Figure 3.11: Load-deflection curves for SFRSCC of different ages

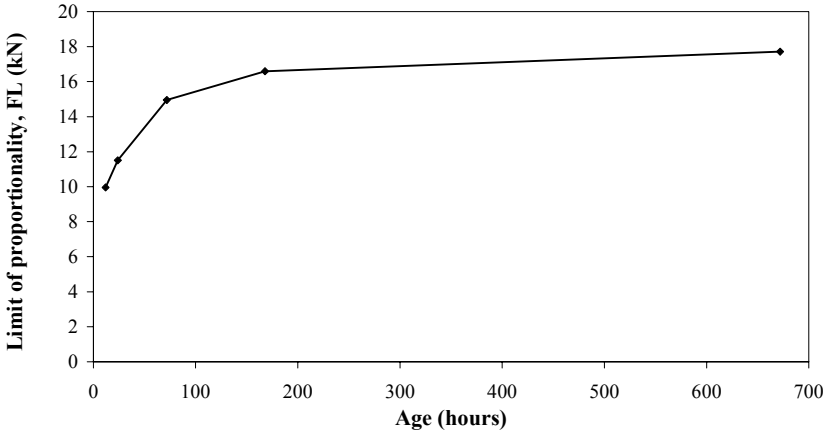

Figure 3.12: Influence of the age in FL

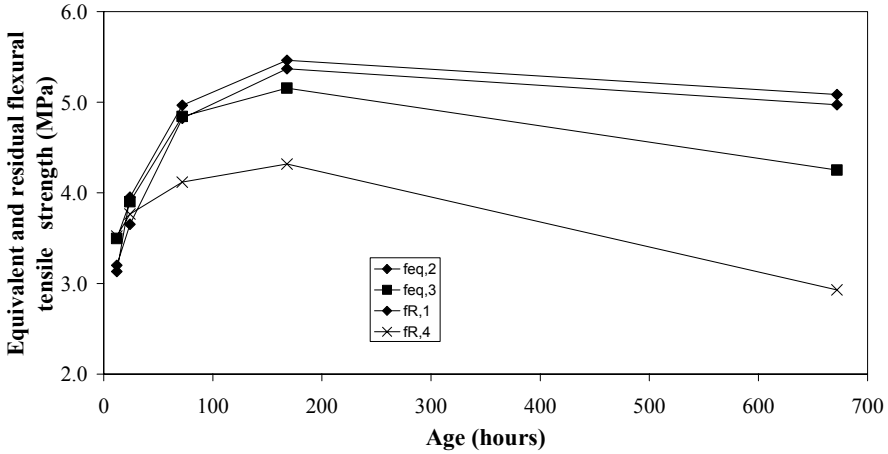

Figure 3.10: Influence of the age in equivalent and residual flexural strength parameters.

3.1.3. Fracture parameters of SFRSCC

Previous research has shown that the post-cracking behavior of SFRC materials can be simulated by the trilinear stress-crack opening diagram, σ-*w*, represented in Figure 3.14 (Vandewalle et al. 2002, Barros et al. 2005). To evaluate the influence of the SFRSCC age on the values of the fracture parameters of this material, an inverse analysis was carried out in order to obtain the dependence of σ_i and w_i, that define the σ-*w* diagram, on the age of the SFRSCC. Knowing these dependencies, the influence of the SFRSCC age on its fracture energy can be directly derived.

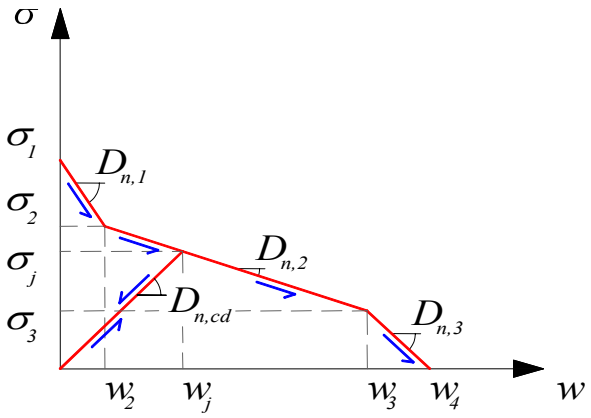

Figure 3.14: Stress-crack opening diagram

The inverse analysis was performed evaluating the σ_i and w_i values that best fit the experimental *F*-δ curves with the minimum error of the parameter,

$$err = \left| A_{F-\delta}^{\exp} - A_{F-\delta}^{num} \right| \Big/ A_{F-\delta}^{\exp} \tag{5}$$

where $A_{F-\delta}^{\exp}$ and $A_{F-\delta}^{num}$ are the areas below the experimental and the numerical *F*-δ curves, respectively. For this purpose, a computational code named FEMIX (Azevedo et al. 2003) was used, that has discrete and smeared crack models to simulate the crack initiation and crack propagation in cement based materials. Since the RILEM TC 162-TDF flexural test brings up a localized fracture problem, a discrete crack model, described in detail elsewhere, was used. Six-node 2D (see Figure 3.15) line interface finite elements were located in the specimen's symmetry axis to model the fracturing process. In the remaining parts of the specimen, eight-node Serendipity linear-elastic plane-stress elements were used. Gauss-Lobatto integration scheme with three integration points (IP) was used for the 2D line interface finite

elements, while Gauss-Legendre integration scheme with 2×2 IP was used for the eight-node elements. To avoid undesired spurious oscillations of the stress field, a value of 1.0×10^4 N/mm^3 was assigned to the initial mode I stiffness for the interface element 3. Since sliding between the fracture surfaces does not occur in this type of problem, the analysis is independent of the values assigned to the mode II stiffness of the interface element.

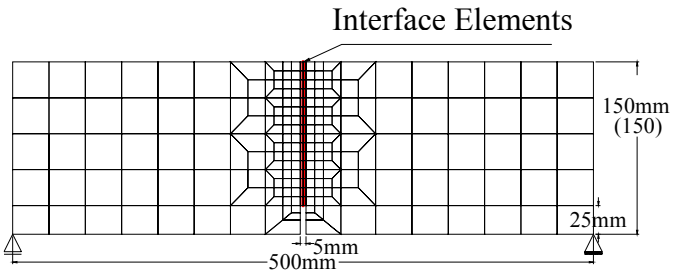

Figure 3.11: Finite element mesh

The adequacy of the numerical strategy adopted is shown in Figure 3.16, revealing that the proposed trilinear σ-*w* diagram is capable of predicting, with enough accuracy, the post-cracking behavior of the tested specimens. The values for σ_i and w_i are included in Table 2 and correspond to the simulation of the average F-δ experimental curves.

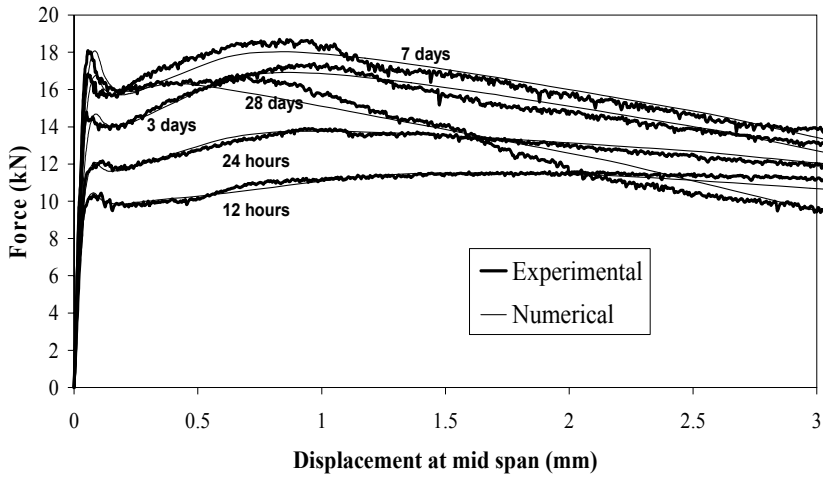

Figure 3.16: Experimental and numerical F-δ curves

Table 3.2: Fracture parameters of SFRSCC with of different ages.

Age (days)	σ_1 (MPa)	w_2 (mm)	σ_2/σ_1	w_3 (mm)	σ_3/σ_1	w_4 (mm)	G_f (N/mm)
0.5	1.52	0.06	0.7	1	0.85	9	6.37
1	1.80	0.06	0.7	0.5	0.88	8	6.62
3	2.25	0.06	0.68	0.5	0.88	5	5.31
7	2.60	0.06	0.65	0.5	0.80	5	5.64
28	2.92	0.06	0.58	0.25	0.62	4	3.90

As Figure 3.17 shows, σ_i increase up to 7 days. After this age, σ_1 continues to increase, σ_2 maintains practically constant, and σ_3 decreases. From Figures 3.18 and 3.19 it seems that the age has a tendency to reduce the values of the w_3 and w_4, while w_2 is not affected by the age of the specimen. This means that the slope of the first softening branch of the σ-w diagram, $D_{n,1}$, increases with the ages, (see Figures 3.14 and 3.20). Similar tendency was observed in the $D_{n,3}$, (see Figures 3.14 e 3.22), but the increase after 3 days was not so pronounced. The variation of the $D_{n,2}$ with the age is represented in Figure 3.21, reflecting a hardening effect of increasing value up to 3 days, followed by a reduced decrement after this age (see Figure 3.11).

The higher inclination of the softening branches and the smaller amplitude of the "hardening" branch of the σ-w diagram of the specimens with 28 days reflect the brittler character of the F-δ response registered in these specimens.

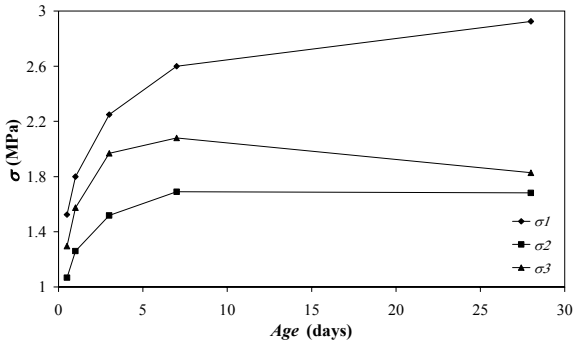

Figure 3.17: Influence of SFRSCC age in σ_i

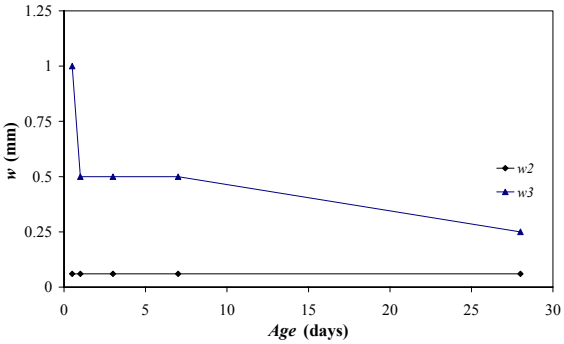

Figure 3.12: Influence of SFRSCC age in $w2$ and $w3$

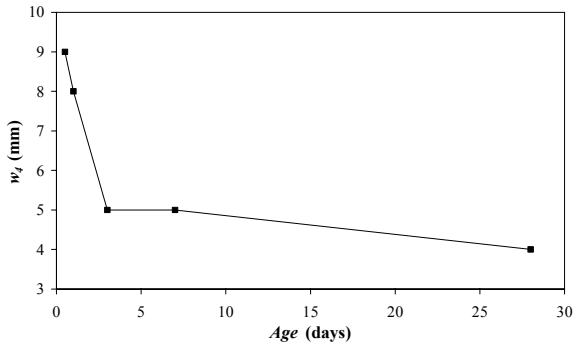

Figure 3.19: Influence of SFRSCC age in w_4.

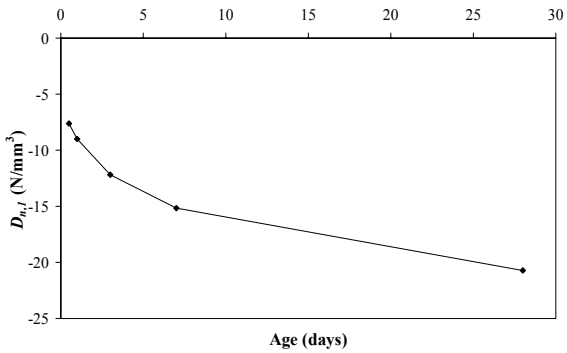

Figure 3.13: Influence of SFRSCC age in parameter $D_{n,1}$

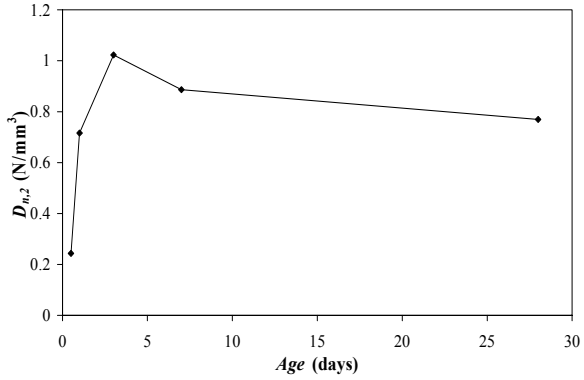

Figure 3.14: Influence of SFRSCC age in parameter $D_{n,2}$.

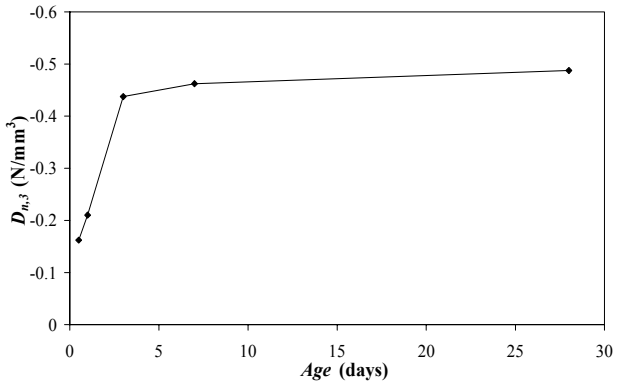

Figure 3.22: Influence of SFRSCC age in parameter $D_{n,3}$.

For modeling the contribution of the fiber reinforcement, the TC 162-TDF recommended the use of $f_{R,4}$ for the ultimate limit state analysis. The $f_{R,4}$ is the stress for a deflection of 3.0 mm. Therefore, only the fracture energy dissipated up to this deflection, $G_{f,3mm}$, has interest from the design point of view. The influence of the SFRSCC age on the evolution of the $G_{f,3mm}$ is represented in Figure 3.23, from which can be concluded that $G_{f,3mm}$ increases up to 7 days, followed by a significant decrease after this age. This means that the fiber reinforcing mechanisms were not sufficiently benefited by the increase of the matrix strength with the age in order to assure the tendency observed in the specimens tested up to 7 days. To avoid the decrease of the $G_{f,3mm}$ after 7 days, a higher content of fibers should be applied.

Figure 3.24 shows that exists an high correlation between σ_1 and $f_{ctk,min}$, having $f_{ctk,min}$ been evaluated according to the Model Code CEB-FIP recommendations (1993).

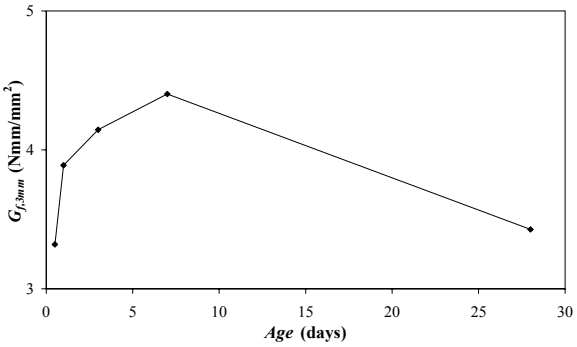

Figure 3.23: Influence of the SFRSCC age on $G_{f,3mm}$.

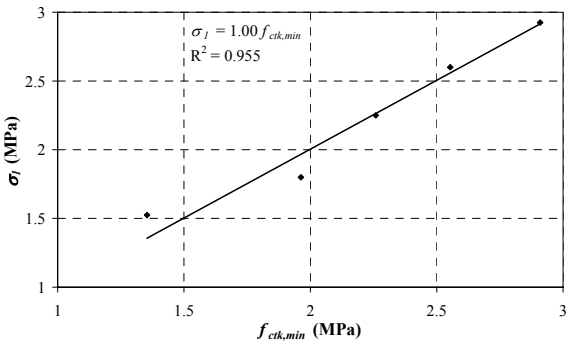

Figure 3.24: Relationship between σ_1 and $f_{ctk,min}$.

According to TC 162-TDF, σ_2 is linearly dependent of $f_{eq,2}$ or $f_{R,1}$, while σ_3 is linearly dependent of $f_{eq,3}$ or $f_{R,4}$. The σ_2-$f_{eq,2}$, σ_2-$f_{R,1}$ and σ_3-$f_{eq,3}$ dependencies are confirmed in Figures 3.25 to 3.27, but Figure 3.28 indicates that a σ_3-$f_{R,4}$ dependence was not assured. The scalar values of the σ_2-$f_{eq,2}$ and σ_3-$f_{eq,3}$ dependencies are, however, distinct to those proposed by TC 162-TDF for the SFRC (0.45 and 0.37, respectively, while 0.32 and 0.40 were obtained for the SFRSCC).

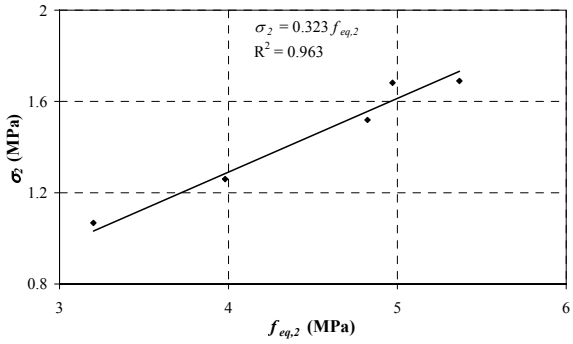

Figure 3.15: Relationship between σ_2 and $f_{eq,2}$

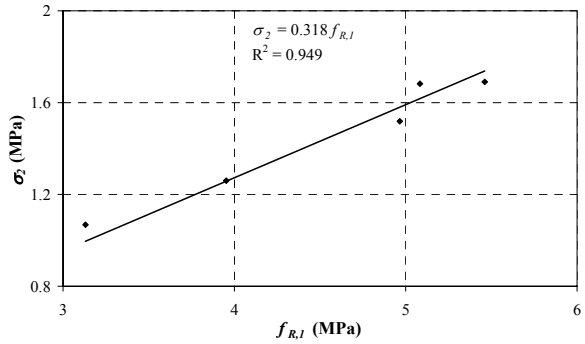

Figure 3.16: Relationship between σ_2 and $f_{R,1}$

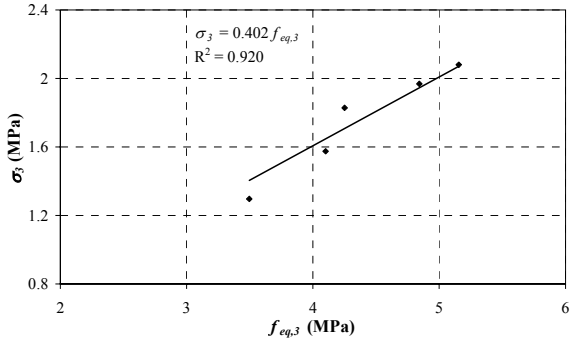

Figure 3.17: Relationship between σ_3 and $f_{eq,3}$.

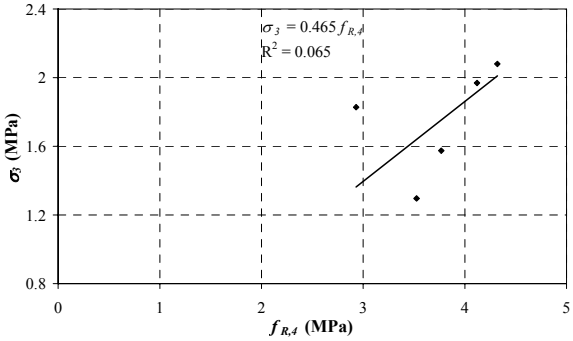

Figure 3.18: Relationship between σ_3 and $f_{R,4}$.

3.1.4. Conclusions

In the present section a method for cost competitive steel fiber reinforced self-compacting concrete (SFRSCC) was described. The developed SFRSCC has attained all the requirements of self-compacting and compression strength of 25 MPa at 12 hours and 62 MPa at 28 days, with a content of cement of about 360 kg/m^3.

To assess the influence of the age on the compression and bending behavior of the developed SFRSCC, an experimental program was carried out, testing specimens at 1/2, 1, 3, 7 and 28 days. The strength and ductility levels required by precasting industry for the application in which the designed SFRSCC will be used, were exceeded. Special research effort was done to assess the influence of the SFRSCC age on the mode I fracture parameters of this material. Taking the force-deflection relationships ($F-\delta$) obtained in the three point bending tests with SFRSCC notched beams and performing an inverse analysis with a discrete crack model, a trilinear stress-crack opening diagram ($\sigma-w$) was obtained for the distinct ages considered.

The obtained $F-\delta$ relationships show that, to maintain the post-cracking residual force up to a deflection of 3 mm, a higher content of fibers should be used (45 kg/m^3 seems to be an adequate fiber content for this purpose). The influence of the SFRSCC age on the σ_i, w_i values defining the $\sigma-w$ diagram was analyzed, as well as, on the corresponding fracture energy. A correspondence between the σ_i values of the $\sigma-w$ diagram and the equivalent and residual flexural tensile strength parameters (f_{eq} and f_R, respectively) proposed by RILEM TC 162-TDF was obtained in order to check the applicability of the post-cracking diagram proposed by this committee for the design of SFRC. A good correlation was obtained between the σ_i and f_{eq} but the constants of this correlation were not equal to those recommended by RILEM TC 162-TDF for the current SFRC. New values were proposed for the developed SFRSCC.

3.2. Experimental Program II – SFRSCC _45

In the Experimental Program I – SFRSCC_30, the obtained $F-\delta$ relationships showed that, to maintain the post-cracking residual force up to a deflection of 3 mm, a higher content of fibers should be used. The shape of the obtained force-deflection relationships, and the accumulated experience in previous research projects in the ambit of SFRC, indicate that an amount of 45 kg/m^3 of fibers could be enough to attain the aforementioned purpose. Therefore, an experimental program, similar to the one described in Section 3.1, was carried out with a SCC reinforced with 45 kg/m^3 of fibers.

3.2.1. Conception method

The materials used in the experimental program for the development of SCC reinforced with 45 kg/m^3 of fibers (SRFSCC_45) were the same of SFRSCC_30. The SFRSCC conception method was the one described in Section 3.11. However, since a higher content of fibers is now used, the solid skeleton composition (aggregates) should be redesigned to avoid an increase of void content in the solid skeleton structure. The solid skeleton composition was evaluated according to the procedures followed for SRFSCC_30. The final composition of the solid skeleton for SRFSCC_45 was (in percentage of volume): 46.75% of coarse sand, 38.25% of crushed aggregate and 15% of fine sand. Note that the percentage of fine sand increased, while the relative percentage of coarse sand and crushed aggregate was maintained.

To obtain the percentage of the binder past in the total volume of concrete, series of experimental castings was made, varying the percentage of binder paste. The self compacting parameters were measured for each trial, performing the L-Box and the Slump Flow tests. In this phase the V-Funnel test was not used. In fact, this test is not feasible since the fiber has a length to high for the reduced overture of the apparatus of this test. Table 3 includes the composition of the SFRSCC_45.

Table 3.3: Final composition to 1 m^3 of SFRSCC with 45kg of fibers

Paste/ Total volume (%)	Cement (kg)	FC (kg)	Water (dm^3)	SP (dm^3)	Fine sand (kg)	Coarse sand (kg)	Crushed stone (kg)
0.38	401.68	344.30	117.31	7.65	178.13	669.36	600.00

3.2.2. Mechanical properties of SFRSCC_45

The experimental program with SFRSCC_45 followed the same procedures of the experimental program with SFRSCC_30. Therefore, the characterization of SFRSCC_45 was also composed by compression tests in cylinders of 150 mm diameter and 300 mm height and bending tests in prismatic 600×150×150mm^3 specimens. Both types of specimens were filled without any compaction. To evaluate the influence of SFRSCC age in the compression and bending behavior, tests with specimens of 0.5, 1, 3, 7 and 28 days were carried out. Tests with lightweight prototypes (bending and punching tests) were also performed.

3.2.2.1. Compression

Figure 3.29 represents the influence of SFRSCC age in the average of the Young's Modulus, E_{cm}, of both SFRSCC_30 and SFRSCC_45. Each E_{cm} value is the average of three specimens for each age. This figure shows that E_{cm} increases with age. At 12 hours SFRSCC_45 had a lower E_{cm} value than the one registered in SFRSCC_30. This can be justified by the distinct temperature of the laboratory environment recorded during the periods of these two experimental programs, which affected the stiffness growing process of the specimens cured in the laboratory environment conditions. In fact, for the SFRSCC_30 the temperature was in the range of 25-28 Celsius degrees while for the SFRSCC_45 the temperature varied from 15 to 17 ^{o}C. At 24 hours, E_{cm} values are of about 27 GPa. After 24 hours the E_{cm} of SFRSCC_30 has a soft increase, and attained 36 GPa at 28 days. The SFRSCC_45 showed a significant increase of E_{cm} between 24 hours and 3 days, having reached 38 GPa at 3 days. After this age, the E_{cm} of SFRSCC_45 increased smoothly, having attained 40 GPa at 28 days.

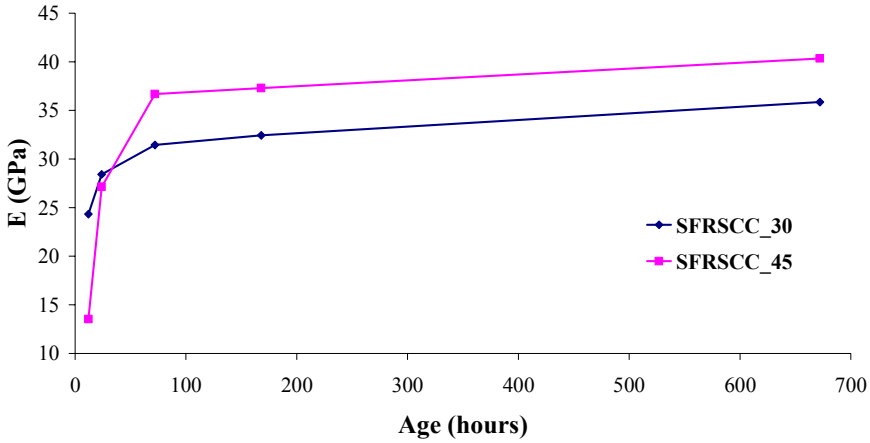

Figure 3.29: Variation of E_{cm} with age.

The stress-strain (σ_c-ε_c) curves obtained for SFRSCC_30 (thinner lines) and SFRSCC_45 (thicker lines) are depicted in Figure 3.30. Apart the ages of 12 h and 24 h, in the remaining testing ages, the compressive strength and the post-peak energy absorption capacity of SFRSCC_45 were larger than the values obtained in the SFRSCC_30. The exceptions are justified by the aforementioned distinct laboratory environmental conditions when the two experimental programs were carried out.

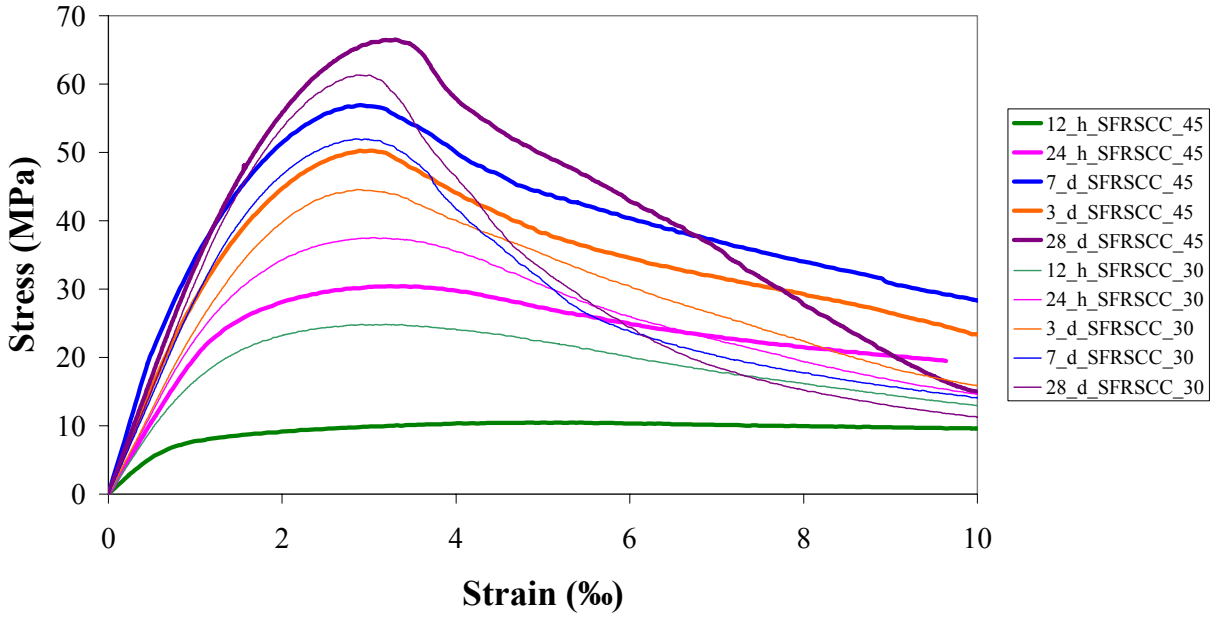

Figure 3.30: Influence of the age on the stress-strain response of SFRSCC_30 and SFRSCC_45

Figure 3.31 represents the influence of SFRSCC age in the values of the average compressive strength, f_{cm}. Due to the reasons already mentioned, at 12 hours the SFRSCC_45 had an unexpected low f_{cm} value. At 24 hours, however, the f_{cm} exceeded the value required by Prégaia Company (20 MPa). At 28 days, the f_{cm} of SFRSCC_45 was 66 MPa, while SFRSCC_30 presented a value of 62 MPa.

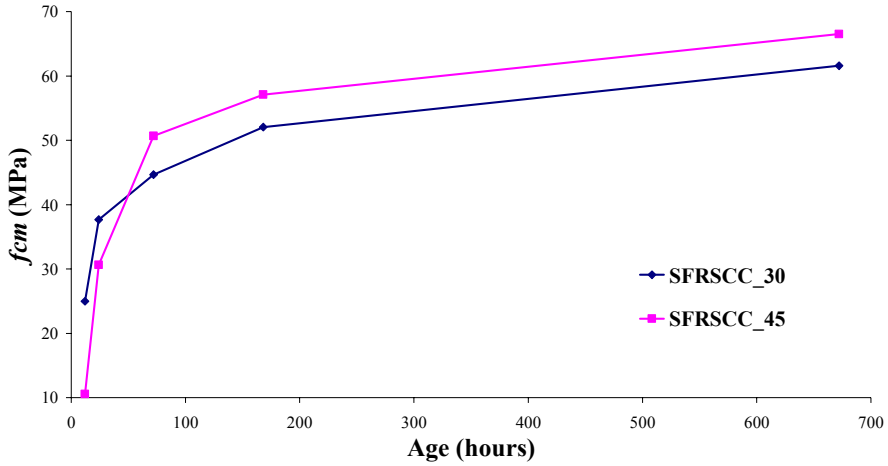

Figure 3.31: Influence of the age on the f_{cm} of SFRSCC_30 and SFRSCC_45

Figure 3.32 shows the typical failure mode occurred in the compression tests, where the confinement provided by the fibers is well evidenced, as well as a good fiber distribution into the concrete.

Figure 3.19: Typical failure mode of compression tests

3.2.2.2. Bending

Figure 3.33 represents the load-deflection curves obtained in SFRSCC_45 specimens of different ages. Figure 3.34 shows the influence of the age in F_L, for both SFRSCC_30 and SFRSCC_45. As expected, apart for 12 hours, due to the reasons already exposed, the differences in the F_L values are not significant, since F_L concept intends to represent the crack initiation of the matrix, which is not too influenced by the presence of the fibers. Analyzing figures 3.33 and 3.34 it is verified that the difference between the maximum force and F_L is much more pronounced in the SFRSCC_45 than in SFRSCC_30, due to the higher fiber content of the former one.

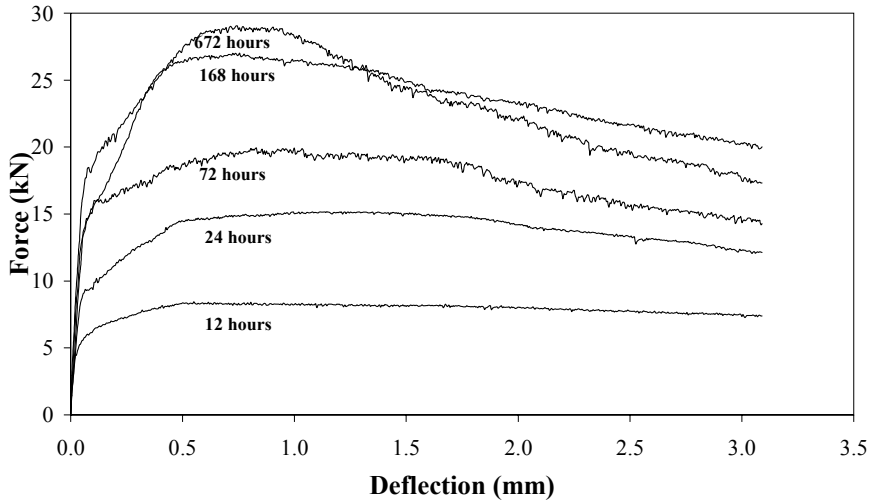

Figure 3.20: Load-displacement curves of SFRSCC_45 specimens of different ages

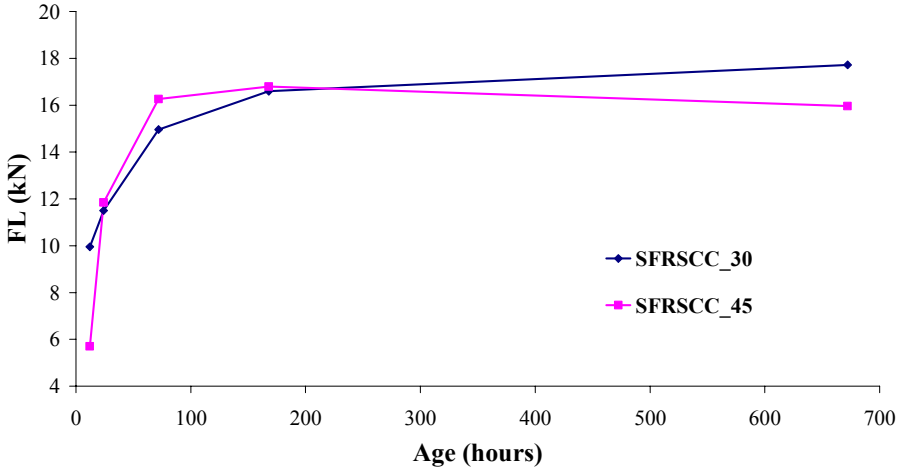

Figure 3.21: Influence of SFRSCC age in FL

Figures 3.35 and 3.36 represent the influence of age the in the equivalent and residual flexural strength parameters. As was expected, the values of these parameters for the SFRSCC_45 are always greater than the values for the SFRSCC_30, except at 12 hours due to the reasons already pointed out. Figure 36 show that, the high f_{eq} values attained in the SFRSCC_45 at 7 days, were maintained up to 28 days, do not having been affected by the influence of the increase of the strength of the material between this two ages, which indicates that 45 kg/m^3 of fibers is an adjusted amount for this purpose.

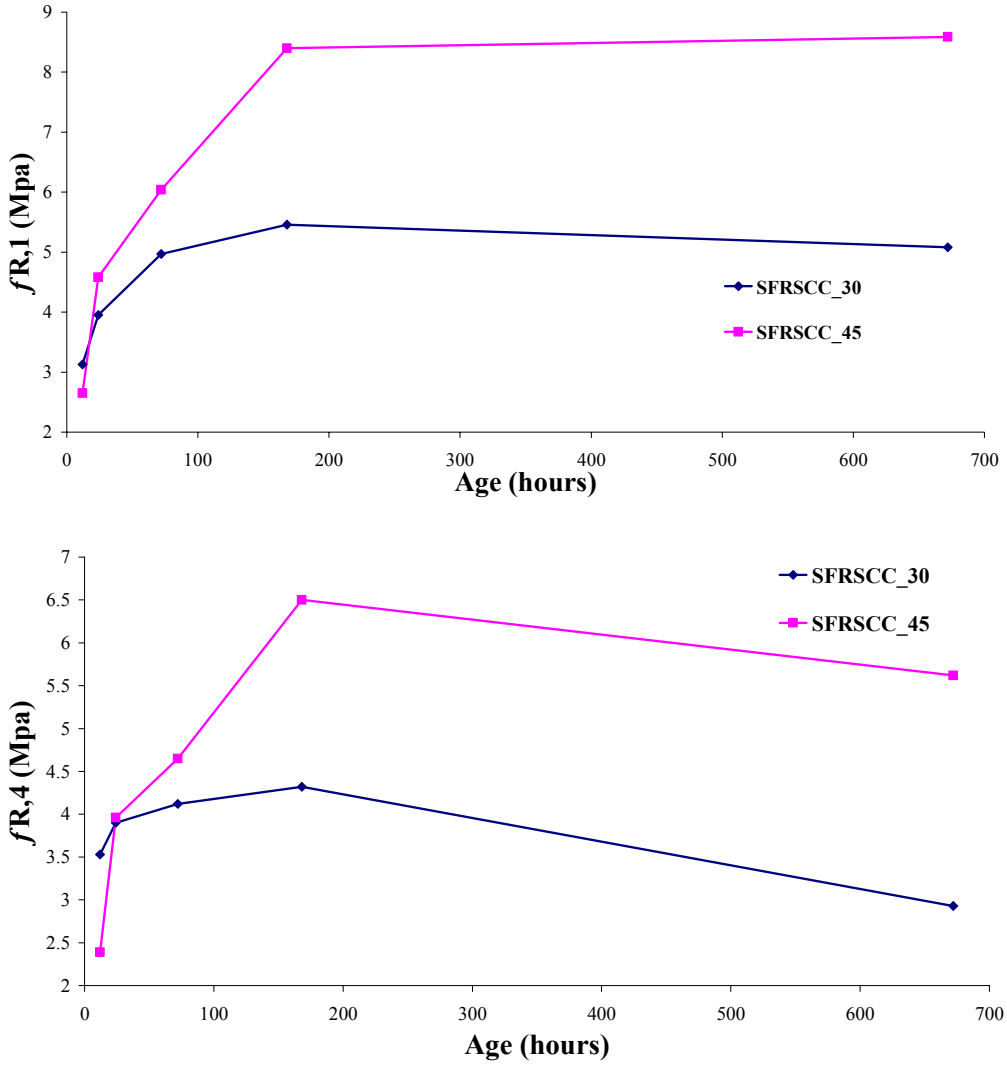

Figure 3.22: Influence of SFRSCC age in $f_{R,1}$ and $f_{R,4}$

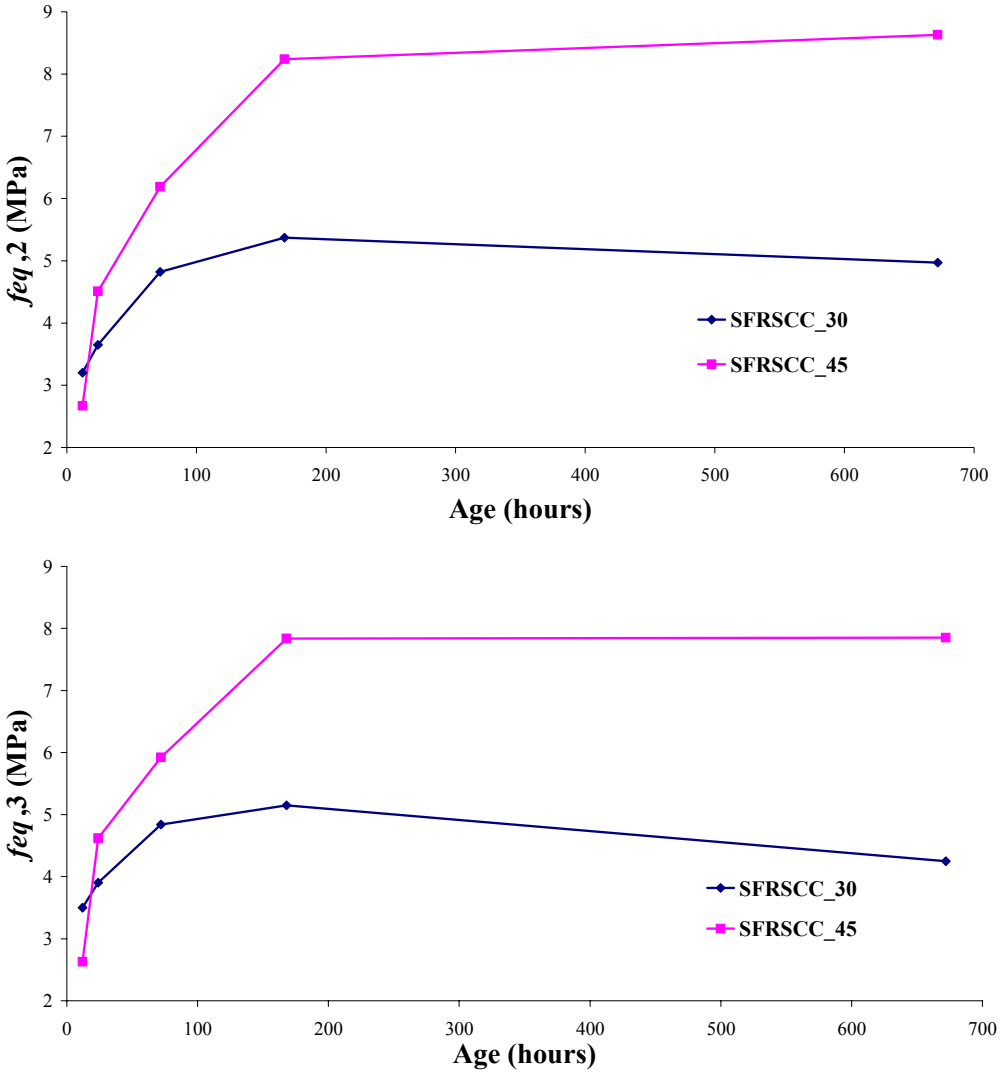

Figure 3.23: Influence of the SFRSCC age in $f_{eq,2}$ and $f_{eq,3}$

3.2.3. Conclusions

Although the f_{cm} values of SFRSCC_45 of 12 h and 24 h were inferior to the ones registered in SFRSCC_30 – fact justified by the significant difference in the temperature of the laboratory environment during the period of execution of the two experimental programs – the values of f_{cm} obtained for the other ages exceeded those of SFRSCC_30. At 28 days, SFRSCC_45 attained an average compressive strength of 66 MPa, with a cement content of about 400 Kg/m^3.

The SFRSCC_45 flexural behavior, evaluated from three point bending notched beam tests carried out according to the RILEM TC 162-TDF recommendations, was significantly more ductile the behavior of SFRSCC_30. These tests showed that an amount of 45kg/m^3 of fibers is capable of maintaining f_{eq} values grater than 7.5 MPa when the strength of the material is almost attained.

4. TESTS IN LIGHTWEIGHT PROTOTYPE PANELS

Having been finished the characterization of the compression and bending behavior of the developed SFRSCC, the next step of the research program is to assess the behavior of SFRSCC panel prototypes under load configurations that can simulate the possible failures modes of the real application where the developed SFRSCC is intended to use: façade panels. Therefore, SFRSCC lightweight panel prototypes were fabricated and tested under load configurations that produce bending and punching failures modes. Bending failures modes can occur due to wind loads. Since the SFRSCC compression layer is only 30 mm thick in the lightweight parts of the panel, punching can occur if point loads act in this part of the panel.

4.1. Panel Geometry

The geometric configuration of the lightweight panel developed is presented in Figure 4.1. The lightweight zones of the panels are constituted by 300x300x80 mm^3 polystyrene blocks, fixed to the formwork by an adhesive, and a massive layer of 30 mm thick. These lightweight parts are involved by massive components forming a grid of bars with 100 mm width and 110mm thick.

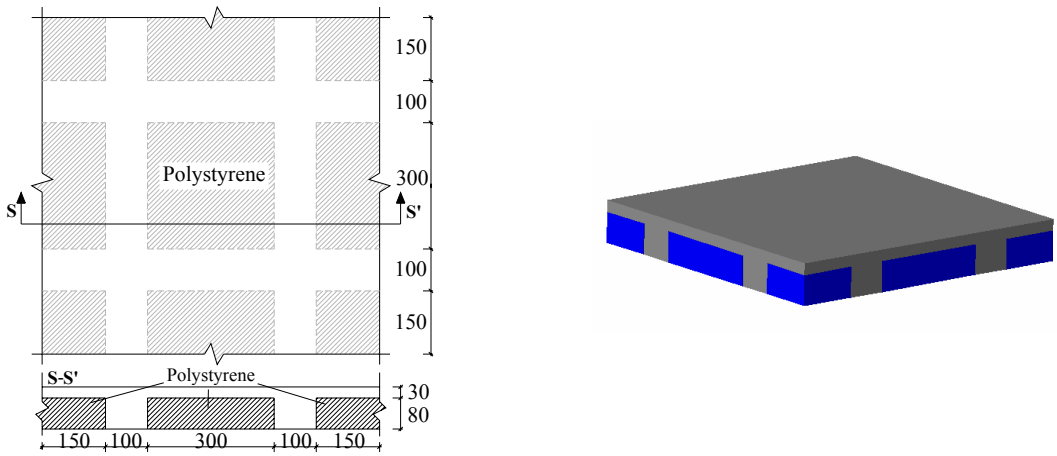

Figure 4.1: Geometry of panel prototype

Panels were filled with the SFRSCC compositions *supra* defined. The concrete was discharged in the center of the formwork, spreading only by its own weight, due to its self-compacting characteristics (see Figures 4.2 to 4.5).

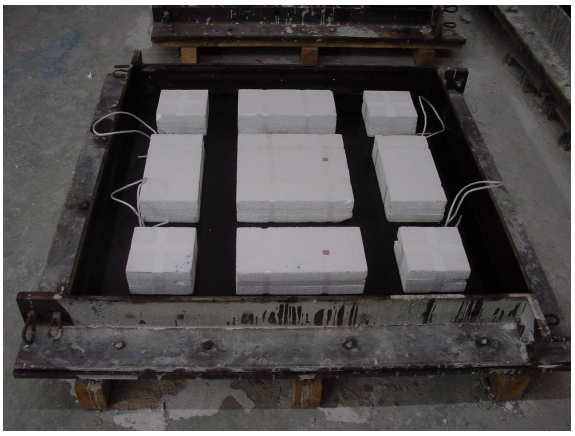

Figure 4.2: Metallic formwork to build the panel and disposition of the lightweight elements

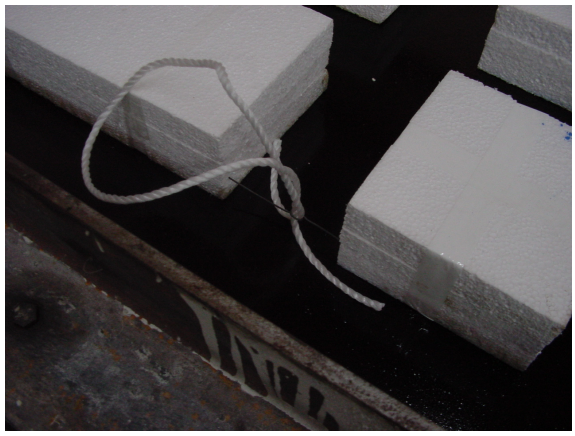

Figure 4.3: Formwork detail

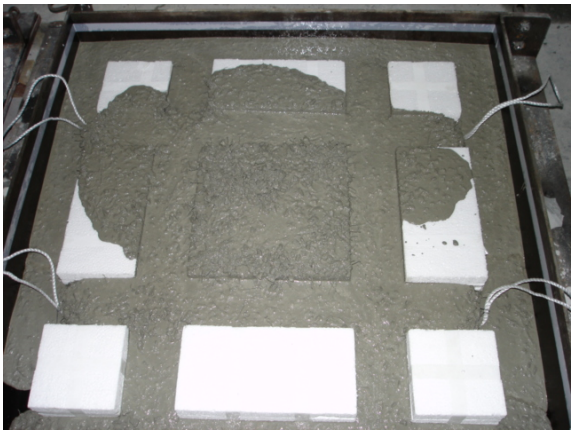

Figure 4.4: Filling the panel

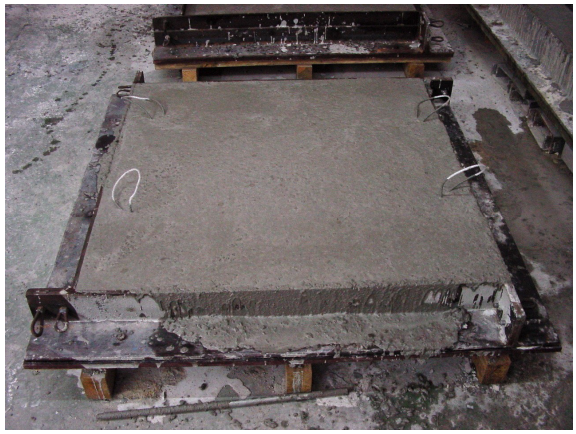

Figure 4.5: Panel after have been cast

4.2. Experimental Program

The experimental program is composed of bending and punching tests in square panels of size edge of 1000 mm and 600 mm, respectively. Both panel series have a thickness of 110 mm. The panels were demolded 24 hours after have been cast, and the tests were carried out at 7 days.

4.3. Bending tests

The test setup of the bending tests with panel prototypes is schematically described in Figures 4.6 to 4.10. The panel has eight supports, each one composed of two square steel plates of 100 mm edge and 10 mm

thick, with a steel sphere of 20 mm diameter between these plates, see Figures 4.6 and 4.7. These supports only avoid displacements in the direction orthogonal to the plane of the panel. The load is applied in four points, using devices similar to those for the supports, see Figure 4.8. A special device was built to transfer the load from the actuator up to these points, which can accommodate the deformation of the panel without introducing parasitic force components in the panel. Four LVDTs were used to measure the deflection of the points at the panel bottom surface, in the alignment of the point loads, see Figure 4.9.

A servo-controlled equipment of maximum load capacity of 500 kN was used. The test was controlled by the displacement transducer of the actuator, at a displacement ratio of 5 μm/s. Figure 4.10 shows a panel prototype being tested in bending.

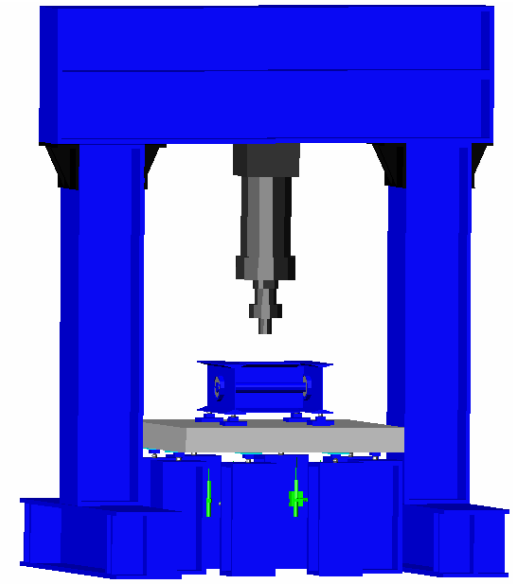

Figure 4.6: Test setup

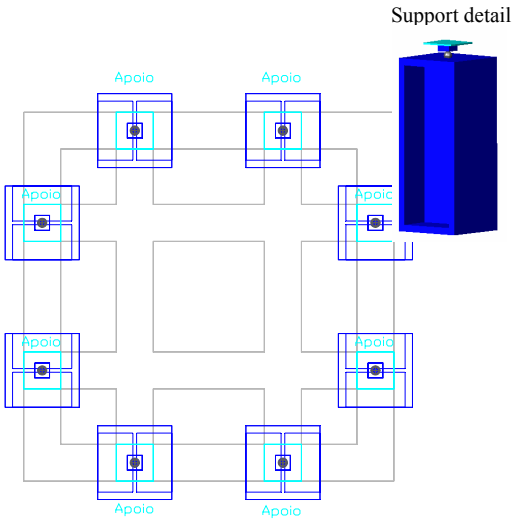

Figure 4.7: Supports of the panel prototype

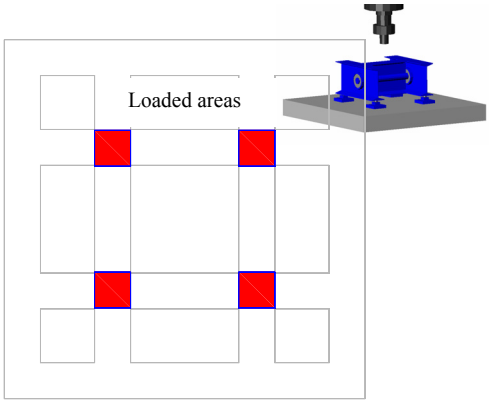

Figure 4.8: Position of the loading points

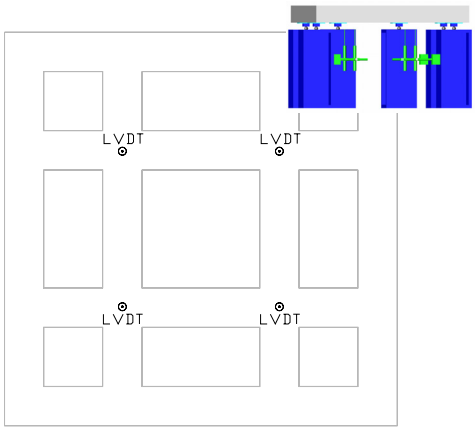

Figure 4.9: Position of the LVDTs to measure the panel deflection

Figure 4.10: Panel prototype being tested in bending

4.3.1. Results

The load-displacement relation recorded in the four LVDTs is represented in Figures 4.11 and 4.12. For both panels the cracking phase starts for a load of about 40 kN. In SFRSCC_30 the load increased until 55 kN, followed by a softening phase. In SRFSCC_45 the increase of the load carrying capacity after crack initiation was much more significant, once a load level of 100 kN was exceeded. Both SFRSCC_30 and SFRSCC_45 panels showed a high residual strength capacity at the post-peak phase. This can only be justified by the reinforcement mechanisms of the fibers bridging the cracks.

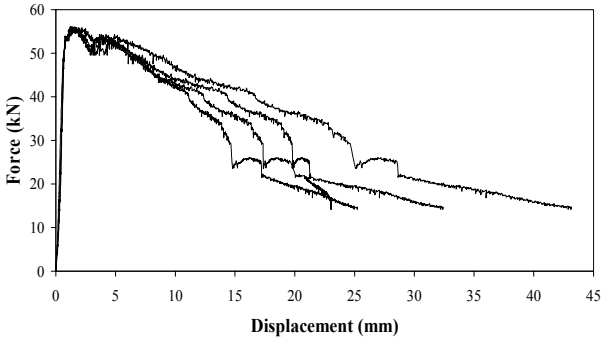

Figure 4.11: Load-deflection curve for each LVDTs of the SFRSCC_30 panel

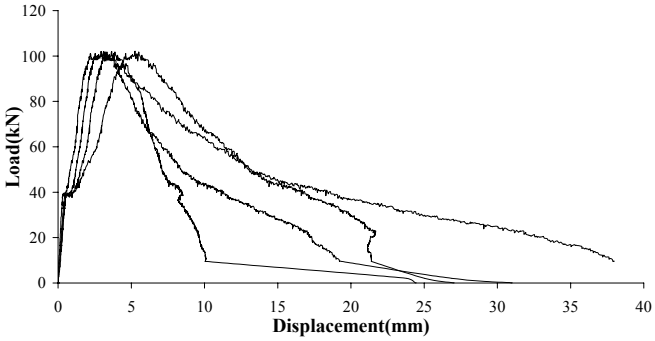

Figure 4.12: Load-deflection curve for each LVDTs of the SFRSCC_45 panel

The typical crack patterns of the tested panels are shown in Figures 4.13 and 4.14. A tendency for a localization of the fracture surfaces near the nodes of the grid can be visualized, due to a stress concentration in these zones.

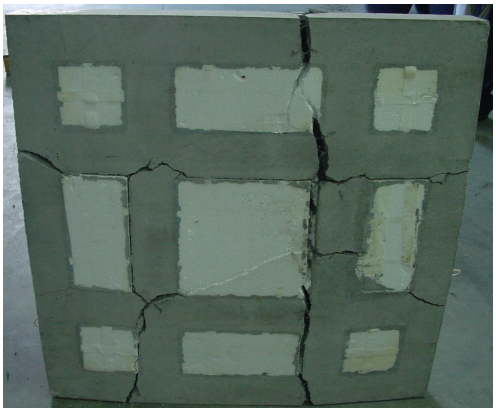

Figure 4.13: Crack pattern in SFRSCC_30, at the end of the bending test

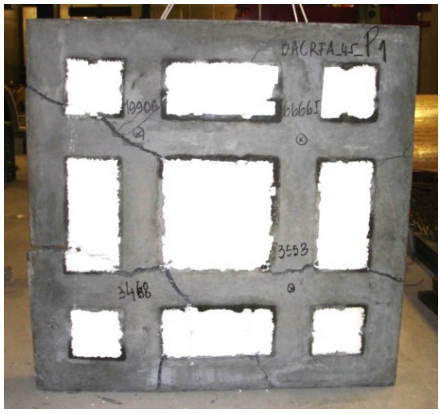

Figure 4.14: Crack pattern in SFRSCC_45, at the end of the bending test

4.4. Punching test

To assess the punching resistance of the lightweight parts of the SFRSCC panels, the panel module shown in Figure 4.15a was tested under the load configuration represented in this figure.

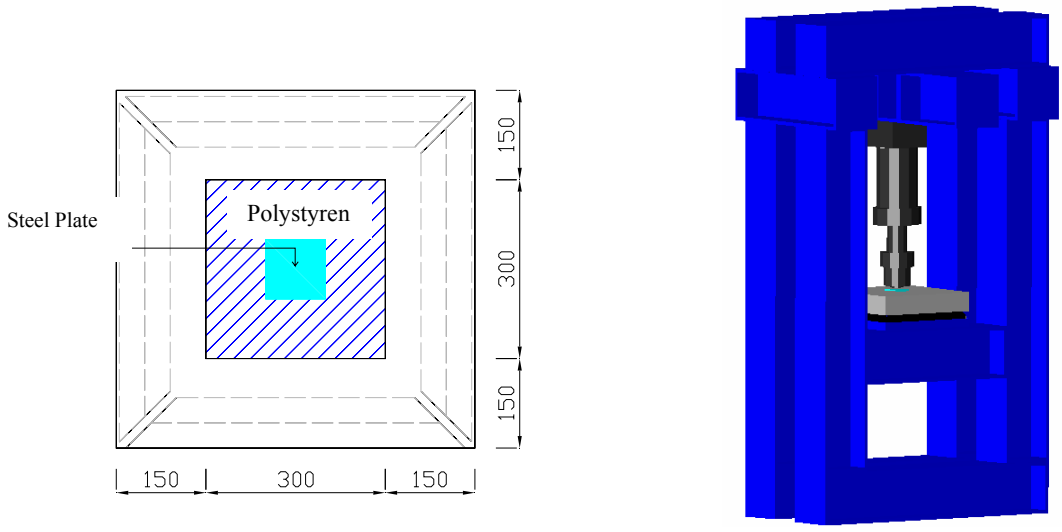

a) b)

Figure 4.155: Setup for the punching tests with panel prototypes

The panel support conditions are represented in Figure 4.16. The panel is simply supported in a steel cylinder forming a square of 500 mm edge (distance between axes). The load applied by the actuator was distributed in a 100x100x10 mm^3 steel plate, and was registered by a cell of 300 kN maximum load

capacity. The test was controlled by the displacement transducer of the actuator, at a deflection ratio of 25 μm/s. The test is ended when a deflection of 30 mm is attained.

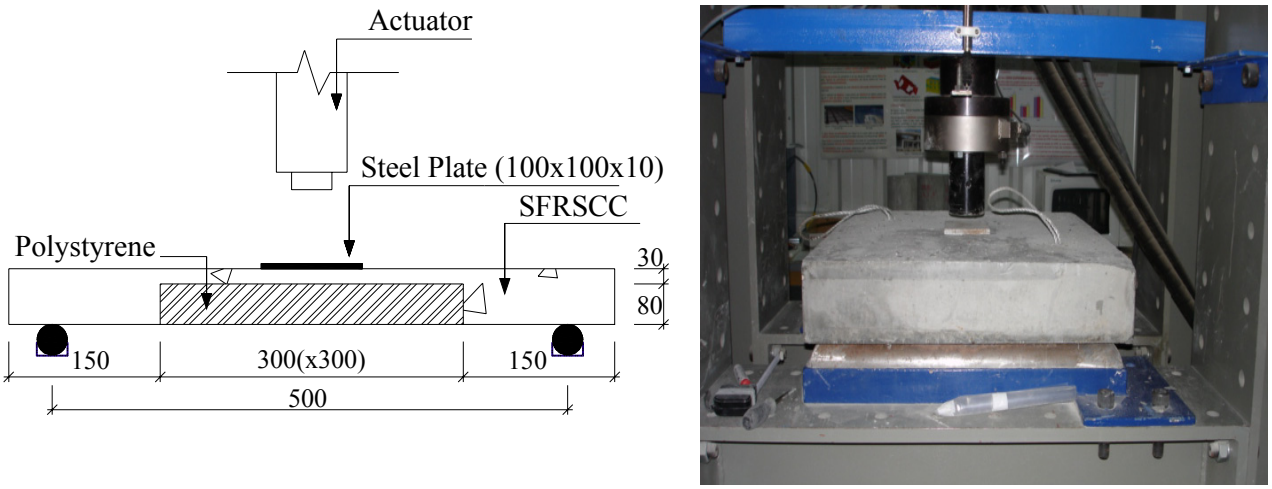

Figure 4.16: Punching test Setup

4.4.1. Results

Figures 4.17 and 4.18 present the relationship between the applied load and the displacement in the LVDT that recorded the penetration of the steel plate into concrete.

Figures 4.17a and 4.18a present the load-displacement relationship up to a displacement of about 10% of the thickness of SFRSCC layer. Up to this deflection the panels have retained their maximum load carrying capacity, which is an indication of the significant stress redistribution capacity provided by fiber reinforcement.

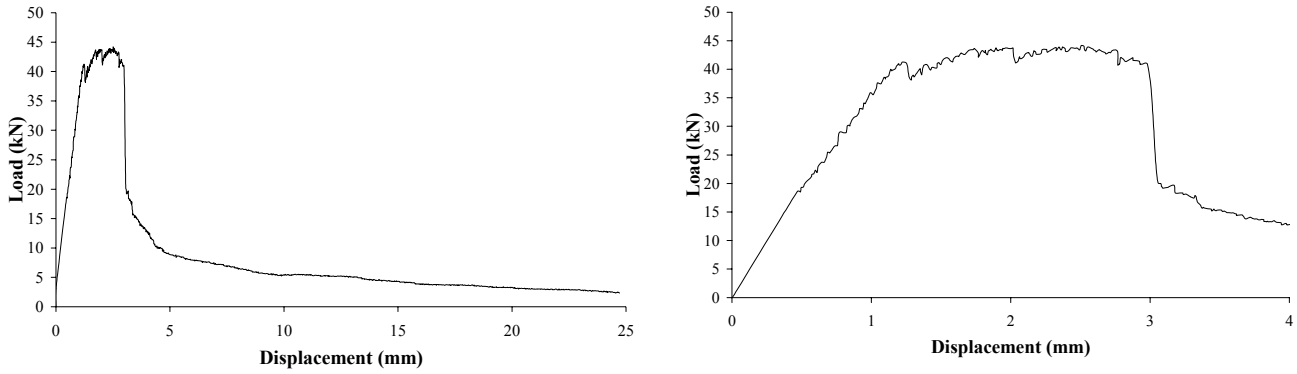

a) b)

Figure 4.17: Load-displacement relationship up to of about a) 20 mm and b) 4 mm, from punching test in a SFRSCC_30 panel

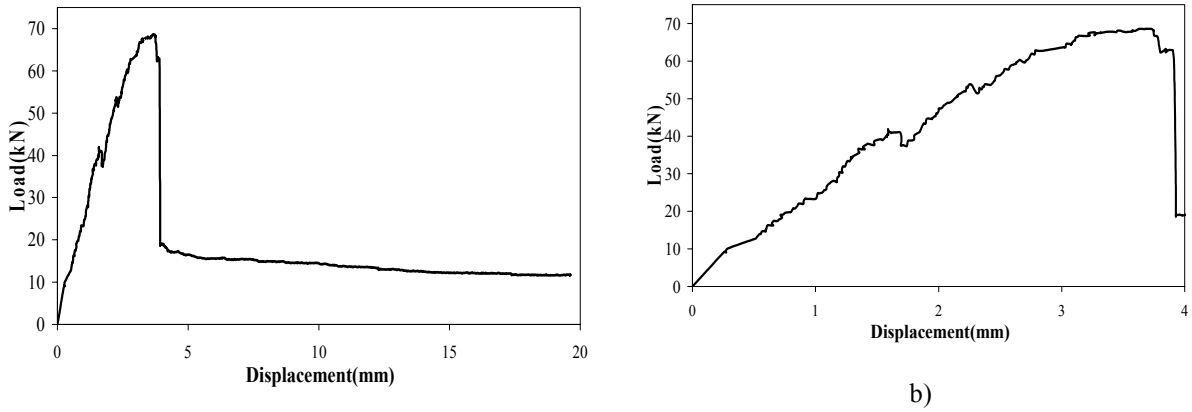

a) b)

Figure 4.18: Load-displacement relationship up to of about a) 20 mm and b) 4 mm, from punching test in a SFRSCC_45 panel

Figure 4.19 shows the typical crack pattern of panels after have been tested. The punching critical contour involves the loaded area at a distance of approximately *d/2*, where *d* is the layer thickness. Due to the resistance provided by fibers bridging the punching failure surface (composed by planes at about 45 degrees - see Figure 4.20), the resistant negative bending moment of the SFRSCC layer was exceeded, leading to the development of a yield line, which is in a middle distance between the punching critical contour and the boundaries of the lightweight part.

Figure 4.19: Punching critical contour and yield line due to negative moments (exterior contour)

Figure 4.20: Failure surface in a punching test

4.5. Conclusions

Bending tests carried out with panel prototypes of the developed SFRSCC showed that the panel structural configuration and the ductility provided by fiber reinforcement allowed high stress redistribution levels, since the maximum load carrying capacity (F_{max}) was much higher that the load a crack initiation (F_{cr}). The load increment, F_{max}-F_{cr}, increased with the content of fibers. After peak load, the panels presented a significant residual load carrying capacity, even at a crack opening several times higher the crack opening limit imposed by the serviceability limit state analysis.

The developed SFRSCC was also very efficient in terms of punching resistance, once the panel maximum load was maintained up to a plate penetration of about 10% of the thickness of SFRSCC layer (30 mm) of the panel lightweight zone.

5. FABRICATION AND TEST OF A REAL PANEL IN INDUSTRIAL ENVIRONMENT

The last phase of the PABERFIA project deals with the fabrication of a real panel in industrial environment. The panel was fabricated in the Prégaia installations, in São Félix da Marinha, Oporto, Portugal. This phase had the aim of verifying if the procedures adopted in the laboratory, in the development of a SFRSCC, can be directly applicable in industrial environment. It had also the purpose of evaluating the behavior of a real panel when submitted to its dead weight and to an increase live load up to its rupture.

The geometry of the fabricated panel is represented in Figure 5.1, which includes extra information related to this panel.

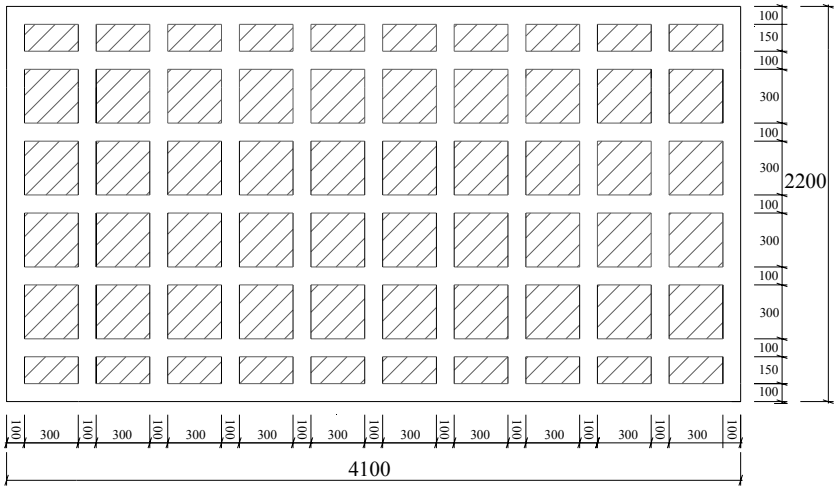

Panel Characteristics	
Width (m)	2.100
Length (m)	4.200
Thickness (m)	0.110
Total Volume(m^3)	0.882
Lightweight (m^3)	0.360
Vol. to cast (m^3)	0.522
Approximate weight (kg)	1305.0

Figure 5.1: Panel Geometry (dimensions in mm)

The panel lightweight parts were materialized by 40 plates of polystyrene plates of 0.30×0.30×0.08 m^3 and 20 plates of 0.30×0.15×0.08 m^3 fixed to timber bars, see Figure 5.2. To maintain this structure stable during the casting process, a very heavy concrete beam was placed on this structure, see Figure 5.3.

Figure 5.2: Placing the lightweight elements

Figure 5.3: Heavy beam to assure stability of the lightweight elements during concrete casting

Two mixtures of 400 dm^3 were made to fabricate the panel and to fill three 0.15×0.15×0.6 m^3 beams and three cylinders of 150 mm diameter and 300 mm height. Slump flow and L-box tests were also carried out to assess the self-compacting characteristics of the designed SFRSCC. Both concrete mixtures were stable without any indication of segregation. The spread was 600 mm and 630 mm in the mixtures 1 and 2, respectively, while the C_{bl} parameter of the L-Box test was 0.80 (the test was only carried out for the second mixture). Figure 5.4 includes a photo of the concrete casting phase.

Figure 5.4: Casting the panel

The demolding of the panel was done in the day after it has been cast, when the SFRSCC had an age of 24 hours. The panel was demolded almost in vertical position (see Figure 5.5).

Figure 5.5: Demolding panel operations

After that, the panel was placed in a support until the test (see Figure 5.6), which occurred at 7 days of panel age.

Figura 5.6: Panel stockage

Figure 5.7 represents the panel support conditions and the location where the deflection was measured (center of the panel). The panel was supported in four points, see Figure 5.8.

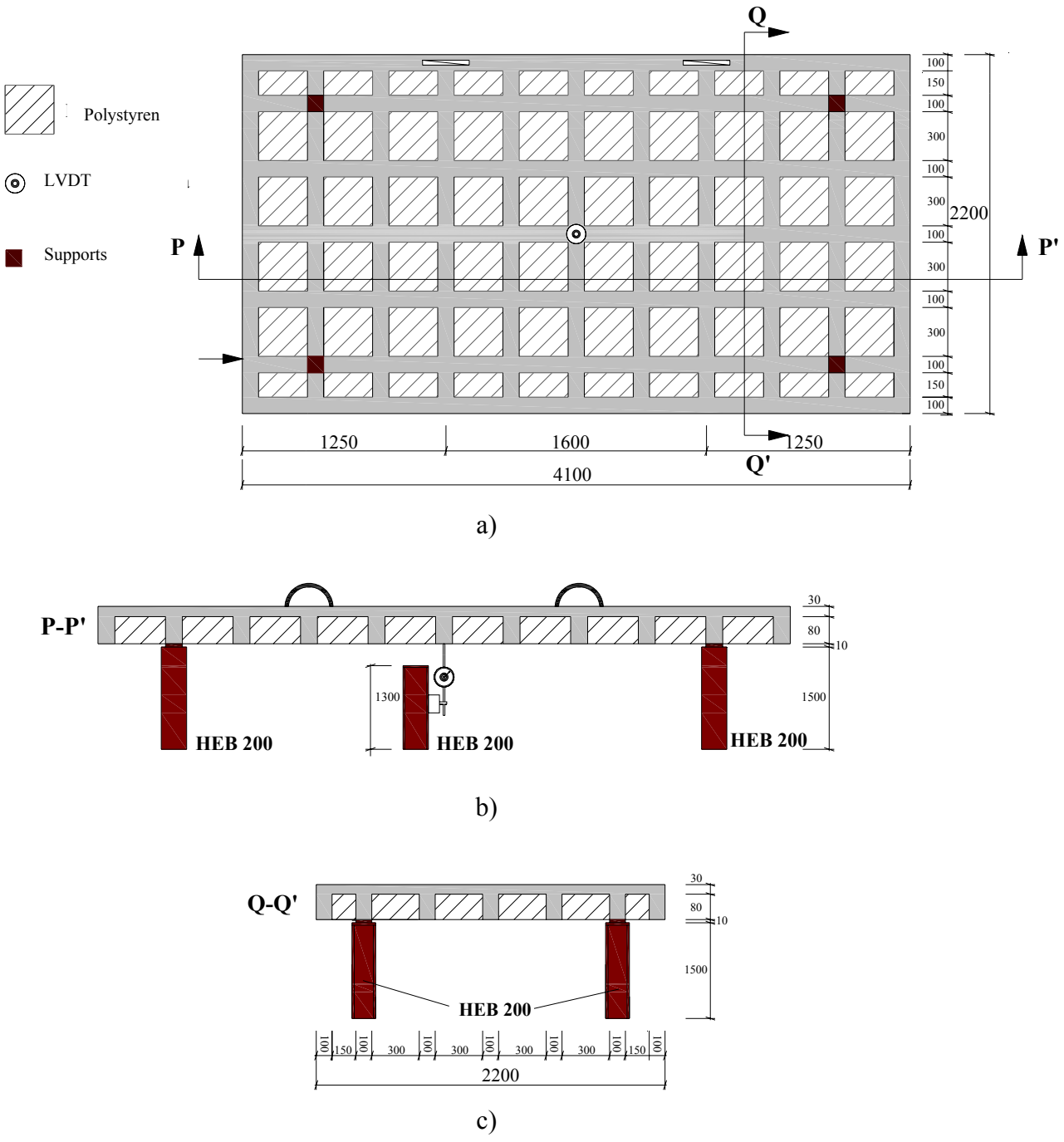

Figure 5.7: Setup of the loading test: a) general view; b) section P-P'; c) section Q-Q'(dimensions in mm)

Figure 5.8: Placing the panel in the supports

A portable data acquisition system (see Figure 5.9), developed by FiberSensing Company, was used to measure the panel deflection at its center, see Figure 5.10.

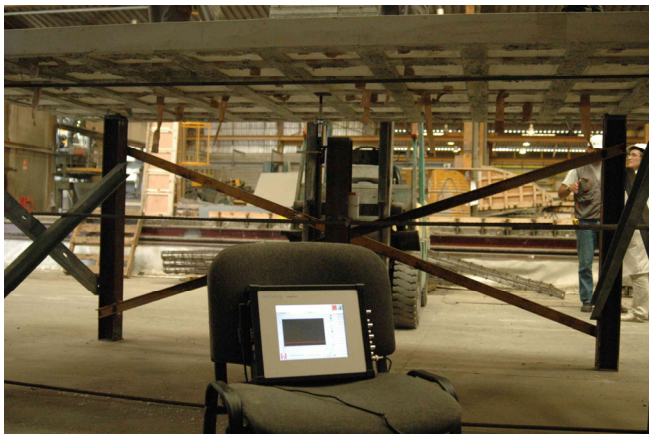

Figure 5.9: Data acquisition system

Figure 5.5: LVDT for measuring the panel deflection at its center

To simulate a uniform distributed live load, concrete plates of 500×500 mm^2, each one of 25 kg, were uniformly distributed in the area interior to the panel supports, see Figure 5.11.

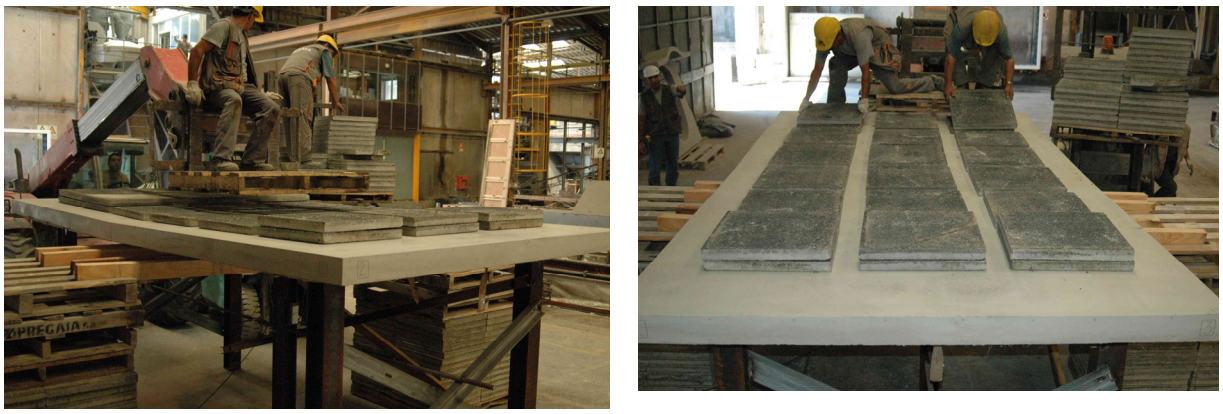

Figure 5.6: Placing the concrete plates to simulate the panel live load

The panel supported 33 concrete plates (see Figure 5.12), corresponding to a uniform distributed load of 8.25/(3.1×1.5)=1.77 kN/m^2, plus its dead weight (1.47 kN/m^2). When placing the 33rd concrete plate, an abrupt increase of deflection occurred, having the test been interrupted due to safety reasons.

Figure 5.7: Final view of the panel, loaded with 33 concrete plates

When the 18th concrete plate was placed, a deflection of 24 mm was measured. When the test was interrupted, the deflection was about 44 mm and the maximum crack opening of the critical crack was around 3 mm. Fibers crossing this crack were visible (see Figure 5.13).

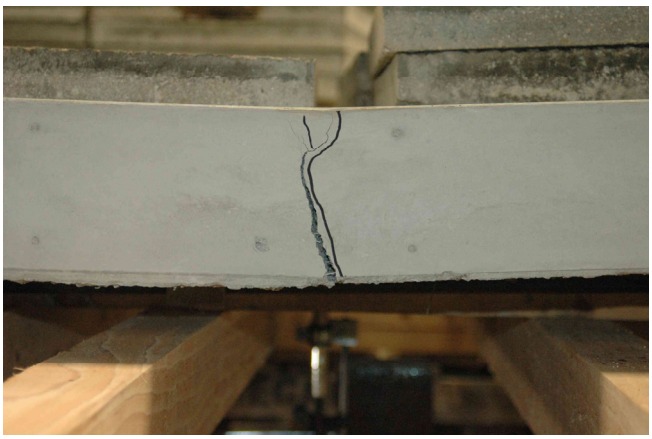

Figure 5.8: Crack opening profile of the critical crack

The total resisted uniform distributed load (1.77+1.47=3.24 kN/m^2) was higher than the characteristic value to the wind dynamic pressure in building with more of 100 m height, located in A zone and in zones of type II irregularity (RSA, 1983). It may be concluded that, for the majority of the buildings, where façade panels are used, the developed SFRSCC_45 panel provides the necessary structural safety.

6. FINAL CONCLUSIONS

A method for conceiving cost competitive steel fiber reinforced self-compacting concrete (SFRSCC) was described. The designed SFRSCC has met all the requirements of self-compactability, and a compressive strength of 25 MPa at 12 hours and 62 MPa at 28 days was reached, with a cement content of about 360 kg/m^3.

To assess the influence of the SFRSCC age on its compression and bending behavior, an experimental program was carried out, testing specimens at 1/2, 1, 3, 7 and 28 days. The strength and ductility levels required by the precasting industry for the application in which the conceived SFRSCC will be used were exceeded. Taking the force-deflection relationships ($F-\delta$) obtained in the three point bending tests with SFRSCC notched beams, and performing an inverse analysis with a discrete crack model, a trilinear stress-crack opening diagram ($\sigma-w$) was obtained for the distinct ages considered. The obtained $F-\delta$ relationships showed that, to avoid a softening phase up to a deflection of 3 mm, a higher fiber content should be used.

The SFRSCC_45 flexural behavior, evaluated from three point bending notched beam tests carried out according to the RILEM TC 162-TDF recommendations, was significantly more ductile than the behavior of SFRSCC_30. These tests showed that an amount of 45kg/m^3 of fibers is capable of maintaining f_{eq} values grater than 7.5 MPa when the strength of the material is almost attained.

The influence of the SFRSCC age on the values of the σ_i, w_i parameters that define the $\sigma-w$ diagram was analyzed. A correspondence between the σ_i values of the $\sigma-w$ diagram and the equivalent and residual flexural tensile strength parameters (f_{eq} and f_R, respectively), proposed by RILEM TC 162-TDF, was obtained in order to verify if the post-cracking diagram proposed by this committee for the design of steel fiber reinforced concrete (SFRC) elements can be applied to the designed SFRSCC. A strong correlation was obtained between σ_i and f_{eq}, but the constants of this correlation were not equal to those recommended by RILEM TC 162-TDF for SFRC. New values were proposed for the designed SFRSCC.

Panel prototypes simply supported on a redundant number of supports were tested up to an average deflection of 30 mm. The maximum force was attained at a deflection of about 0.5 mm, and was maintained up to a deflection of 5 mm, showing that the panel system has high ductility. Beyond this deflection limit, the panel load carrying capacity decreased smoothly.

To assess the punching strength of the lightweight parts of the panel system, panel prototypes were submitted to a punching failure load configuration. A punching crack was formed at the contour of the steel loaded plate, followed by a flexural crack at the borders of the lightweight zone. This second crack, caused by negative moments, was responsible for the quasi-plastic response of the panels up to a penetration of the loaded plate of about 10% of the layer thickness.

The fabrication of the real panel permitted to assess the applicability of SFRSCC to industrial production. It was very useful to verify the concrete behavior in terms of self compacting properties, what permits the adjusting of the necessary parameters to use this concrete in the production line of the promoter company of the project. It was possible to verify the final aspect of panels, due to the usage of a self compacting concrete. In fact the visual appearance was very satisfactory, although some aspects can be improved. The load test was, willfully realized in the most unfavorable way: note that these elements will be placed in vertical plane and not in horizontal plane as this test was performed. The tested panel resisted to its own weight and to an overload of about 1.77 kN/m^2, indicating that it have sufficient structural properties to resist to wind actions that, jointly with demolding, is the most unfavorable.

7. FUTURE DEVELOPMENT PERSPECTIVS

The developed SFRSCC have shown excellent properties of ductility and resistance, with a competitive cost of fabrication. The applications where this material has technical and economic advantages are many; however it is more adequate to be used in structures where the high geometric complexity increase significantly the usage of usual reinforcement and, simultaneously, have a redundant number of supports, in order to profit the reinforcing mechanisms after the starting of matrix cracking. Shells are included in this type of structures (ETARs totally or partially buried structures).

However, the durability properties of this material may be studied. In the case of PABERFIA project, it will be now necessary to develop a system to induce the lightweight in the panel. This system must be implemented in the fabrication line of the company, must be reusable, must have automat characteristics and use eco-efficient and low cost materials. These are the indispensable items to turn the developed material and structural system rentable.

8. REFERENCES:

Azevedo, A.F.M.; Barros, J.A.O.; Sena-Cruz, J.M.; Gouveia, A.V., "Software no ensino e no projecto de estruturas", III Congresso Luso Moçambicano de Engenharia, pp. 81-92, 19-21 Agosto 2003.

Barros, J.A.O., Cunha, V.M.C.F., Ribeiro, A.F., Antunes, J.A.B.; "Post-Cracking Behaviour of Steel Fibre Reinforced Concrete", *RILEM Materials and Structures Journal*, 38(275), p. 47-56, 2005.

Bartos, P.J.M. and Grauers, M., "Self-Compacting Concrete", Concrete, Vol.33, Nº4, 1999

Brite-EuRam programme: BE96-3801/BRPR-CT96-0366, 'Rational production and improved working environment through using self-compacting concrete'.

CEB-FIP Model Code. Comite Euro-International du Beton, Bulletin d'Information nº 213/214, 1993.

Especificação do LNEC E397-1993, "BETOES – Determinação do Módulo de Elasticidade em Compressão", LNEC, Portugal; Maio 1993.

Okamura, H. and Ouchi, M., "Self-Compacting Concrete. Development, Present use and Future", Proc. 1st International RILEM Symposium on Self-Compacting Concrete (Stockholm, Sweden), A. Skarendhal and O.Pstersson (editors), RILEM Publications S.A.R.L, 1999

Gomes, P.C.C. (2002), "Optimization and characterization of high-strength self-compacting concrete", PhD thesis, UPC, Barcelona, Spain.

V.S. Gopalaratnam *et al.*, "Fracture toughness of fiber reinforced concrete", *ACI Materials Journal*, 88(4), 339-353, July-August, 1991.

Hordijk, D.A., "Local approach to fatigue of concrete", Dissertation, Delft University of Technology, 1991.

Petersson et al.,"A Model of Self-Compacting Concrete." Proc. International RILEM Conference on Production Methods and Workability of Concrete, P.J.M Bartos, D.L.Marrs and D.J. Cleand (editors), E&FN Spon, 1996

Rooney, M., Bartos, P.M.J., 'Development of the settlement column segregation test for fresh self-compacting concrete (SCC)', Second International Symposium on SCC, Tokyo, Japan (2001).

RSA, Regulamento de Segurança e Acções para Estruturas de Edifícios e Pontes; Decreto-Lei Nº.235/83 de 31 de Maio

Vandewalle, L. *et al*., "Test and design methods for steel fiber reinforced concrete. Recommendations for bending test", Materials and Structures, V. 33, No 225, pp. 3-5, Jan.-Feb. 2000.

Vandewalle, L. et al., "Test and design methods for steel fiber reinforced concrete. Recommendations for σ-ε design method", Materials and Structures, V. 33, No 226, Mar-Apr., pp. 75-81, 2000.

Vandewalle, L. et al., "Design of steel fibre reinforced concrete using σ-w method: principles and applications", *Materials and Structures Journal*, 35, p. 262-278, June 2002.

Vandewalle, L. *et al*., "Test and design methods for steel fibre reinforced concrete - Final Recommendation", Materials and Structures, V. 35, No 253, pp. 579-582, Nov. 2002.